Environmental Chemistry Letters (2022) 20:3837–3859
https://doi.org/10.1007/s10311-022-01453-6

REVIEW

Bifunctional catalysts for heterogeneous electro-Fenton processes: a review

Yuanyuan Yao[1] · Yuqi Pan[1] · Yanxi Yu[1] · Zixun Yu[1] · Leo Lai[1] · Fangzhou Liu[1] · Li Wei[1] · Yuan Chen[1]

Received: 27 December 2021 / Accepted: 19 April 2022 / Published online: 18 May 2022

Abstract

Fenton processes allow to degrade and mineralize toxic organic contaminants, yet classical Fenton processes require continuously adding hydrogen peroxide and ferrous ions, costly solution pH adjustment, and treatment of secondary iron sludge pollution. Heterogeneous electro-Fenton processes deliver oxidizing radicals with only oxygen and electricity consumed. Bifunctional catalysts allow the synthesis and activation of hydrogen peroxide simultaneously, eliminate additional chemical reagents, and yield no metal residues in treated water. Here, we review bifunctional catalysts for heterogeneous electro-Fenton processes. We describe the mechanisms of oxidizing radical generation from oxygen. Then, we compare different types of bifunctional catalysts based on their elemental compositions: (1) metal/carbon composite catalysts, i.e., monometallic iron/carbon composite catalysts, bimetallic/trimetallic carbon composite catalysts, and transition metal single-atom catalysts; (2) metal composite catalysts without carbon; and (3) metal-free carbon catalysts. Then, we present five other approaches beyond electrocatalysts, which have been used to improve the performance of heterogeneous electro-Fenton processes.

Keywords Heterogeneous electro-Fenton processes · Bifunctional electrocatalyst · Hydrogen peroxide synthesis · Hydrogen peroxide activation · Advanced oxidation processes · Organic contaminants

Introduction

Water pollution is a critical environmental challenge in the world. Every year, large amounts of toxic organic contaminants from personal care products, pesticides, dyes, and antibiotics are released to the environment via industrial, agricultural, and domestic wastewater (Dsikowitzky and Schwarzbauer 2014; Caban and Stepnowski 2021). They cannot be effectively degraded and mineralized by conventional wastewater treatment processes. Additional treatment steps are required to eliminate them, such as adsorption (Wang and Wang 2019), membrane separation (Chong et al. 2010; Mohammad et al. 2015), and advanced oxidation processes (Pignatello et al. 2006). Advanced oxidation processes rely on in situ generated reactive oxygen species to degrade and mineralize organic contaminants (Liu et al. 2021a). For example, hydroxyl radicals (·OH) with a redox potential of 2.8 V can non-selectively oxidize most organic compounds. Among various advanced oxidation processes, such as sonochemical oxidation (Montoya-Rodríguez et al. 2020), photocatalytic oxidation (Serpone et al. 2017), and electrochemical oxidation (Garcia-Segura and Brillas 2011), Fenton processes are relatively simple, in which Fenton reagents (e.g., ferrous ion (Fe^{2+})) react with hydrogen peroxide (H_2O_2) to generate reactive oxygen species (Brillas et al. 2009; Hussain et al. 2021).

In conventional homogenous Fenton processes, external H_2O_2 and Fe^{2+} must be added to the wastewater at the optimal pH of around 3. The cost of H_2O_2, the safety associated with handling, transportation, and storage of high concentration explosive H_2O_2, and the treatment of resulting iron sludge ($Fe(OH)_3$) as reaction waste products bring significant drawbacks. The electro-Fenton process was first reported in the early 2000s (Oturan et al. 2000, 2009; Sirés et al. 2014). H_2O_2 is synthesized in situ by the oxygen reduction reaction and then activated to yield reactive oxygen species. In homogenous electro-Fenton processes, the addition of Fe^{2+} is required, still resulting in Fe sludge. In heterogeneous electro-Fenton processes, Fe species are anchored in heterogeneous iron

✉ Yuan Chen
yuan.chen@sydney.edu.au

[1] The University of Sydney, School of Chemical and Biomolecular Engineering, Darlington, NSW 2006, Australia

catalysts, which minimizes the leaching of free Fe^{2+}, significantly reducing iron sludge generation. They can also work under a wider pH conditions than homogenous processes. Further, heterogeneous electro-Fenton processes often consume less H_2O_2 per mole contaminant degraded. However, their reaction rate is usually much slower than homogenous electro-Fenton processes. Both H_2O_2 synthesis and its activation strongly influence the efficiency of heterogeneous electro-Fenton processes in degrading target contaminants.

Several recent review articles have discussed the development of Fenton and electro-Fenton processes. For example, He and Zhou summarized mechanisms and kinetic models of electro-Fenton processes. They also discussed the effects of critical parameters, including electrode materials, H_2O_2, Fe^{2+}, and contaminant concentrations, pH, electrolyte, current density, O_2 supply rate, temperature, and distance between electrodes (He and Zhou 2017). Wang et al. systematically summarized three routes to generate H_2O_2 from O_2 by various chemical, electrocatalytic, and photocatalytic reactions and their mechanisms. They also discussed the applications of such methods in the degradation of some emerging contaminants (Liu et al. 2021c). Pi et al. (2020) summarized some catalysts used for H_2O_2 generation and activation, such as zero-valent metals and Fe^{2+} species used for O_2 reduction, noble metals used for H_2-enabled reactions, as well as photocatalysts. Further, metal–organic framework-derived catalysts (Cheng et al. 2018), graphene-based catalysts (Divyapriya and Nidheesh 2020), and single-atom catalysts (Shang et al. 2021) used in electro-Fenton processes have also been reviewed. The synthesis and activation of H_2O_2 can be catalyzed on a single catalyst (a bifunctional catalyst) or two different catalysts. Bifunctional catalysts can selectively and efficiently catalyze both reactions, bringing significant benefits for practical applications. The recent development of bifunctional catalysts for heterogeneous electro-Fenton processes has not been reviewed to the best of our knowledge.

Here, we review recent advances of bifunctional catalysts used for the in situ electrocatalytic synthesis of H_2O_2 and the activation of H_2O_2 to yield reactive oxygen species. First, we discuss current mechanistic understandings on H_2O_2 synthesis by electrochemical oxygen reduction reaction and the activation of H_2O_2 to generate reactive oxygen species. Next, we summarize different bifunctional catalysts explored in heterogeneous electro-Fenton processes, including metal/carbon composite catalysts, metal composite catalysts without carbon, and metal-free carbon catalysts. We further introduce some other performance improvement approaches. Last, we provide our perspectives on the future development of more efficient bifunctional catalysts. We hope this review can serve as a helpful guide and reference to mechanistic understandings and the latest development of bifunctional catalysts used in heterogenous electro-Fenton processes.

Transformation of O_2 into reactive oxygen species

The chemical reactions in electro-Fenton processes involve two critical steps. The first is the in situ synthesis of H_2O_2 from O_2 by electrochemical oxygen reduction reaction. The second is the activation of H_2O_2 to generate reactive oxygen species, such as $^{\cdot}OH$, $^{\cdot}O_2^-$, or to generate high-valent Fe-oxo species (Fe^{IV}). These reactive oxygen species would further react with organic contaminant molecules, leading to their degradation. We discuss current mechanistic understandings of these two critical steps in the following two subsections.

Synthesis of H_2O_2 by dioxygen reduction

Electro-Fenton processes often take place in acidic aqueous solutions. As illustrated in Fig. 1a, electrochemical oxygen reduction reaction in acidic media may proceed via three possible reaction pathways. In associate oxygen reduction reaction, O_2 is first adsorbed on an active catalytic site (*) (Eq. 1), followed by taking a proton and electron pair from the cathode to form a reaction intermediate (*OOH) (Eq. 2). Afterward, *OOH may take one more proton and electron pair and then desorb from the active catalytic site as an H_2O_2 molecule in the 2 e^- pathway (Eq. 3). Equation 4 is the overall reaction formula. Alternatively, *OOH can be reduced to two H_2O molecules in three steps (Eq. 5–7) by accepting three more proton and electron pairs in the 4 e^- pathway. Equation 8 is the overall reaction formula. Alternatively, in dissociative oxygen reduction reaction, O_2 first directly dissociates (Eq. 9) on two active catalytic sites (*), yielding two *O reaction intermediates. Then, *O proceeds to H_2O (Eq. 6–7).

$$O_2 + * \rightarrow {}^*O_2 \tag{1}$$

$${}^*O_2 + H^+ + e^- \rightarrow {}^*OOH \tag{2}$$

$${}^*OOH + H^+ + e^- \rightarrow H_2O_2 + * \tag{3}$$

$$O_2 + 2\left(H^+ + e^-\right) \rightarrow H_2O_2 \tag{4}$$

$${}^*OOH + H^+ + e^- \rightarrow {}^*O + H_2O \tag{5}$$

$${}^*O + H^+ + e^- \rightarrow {}^*OH \tag{6}$$

$${}^*OH + H^+ + e^- \rightarrow H_2O + * \tag{7}$$

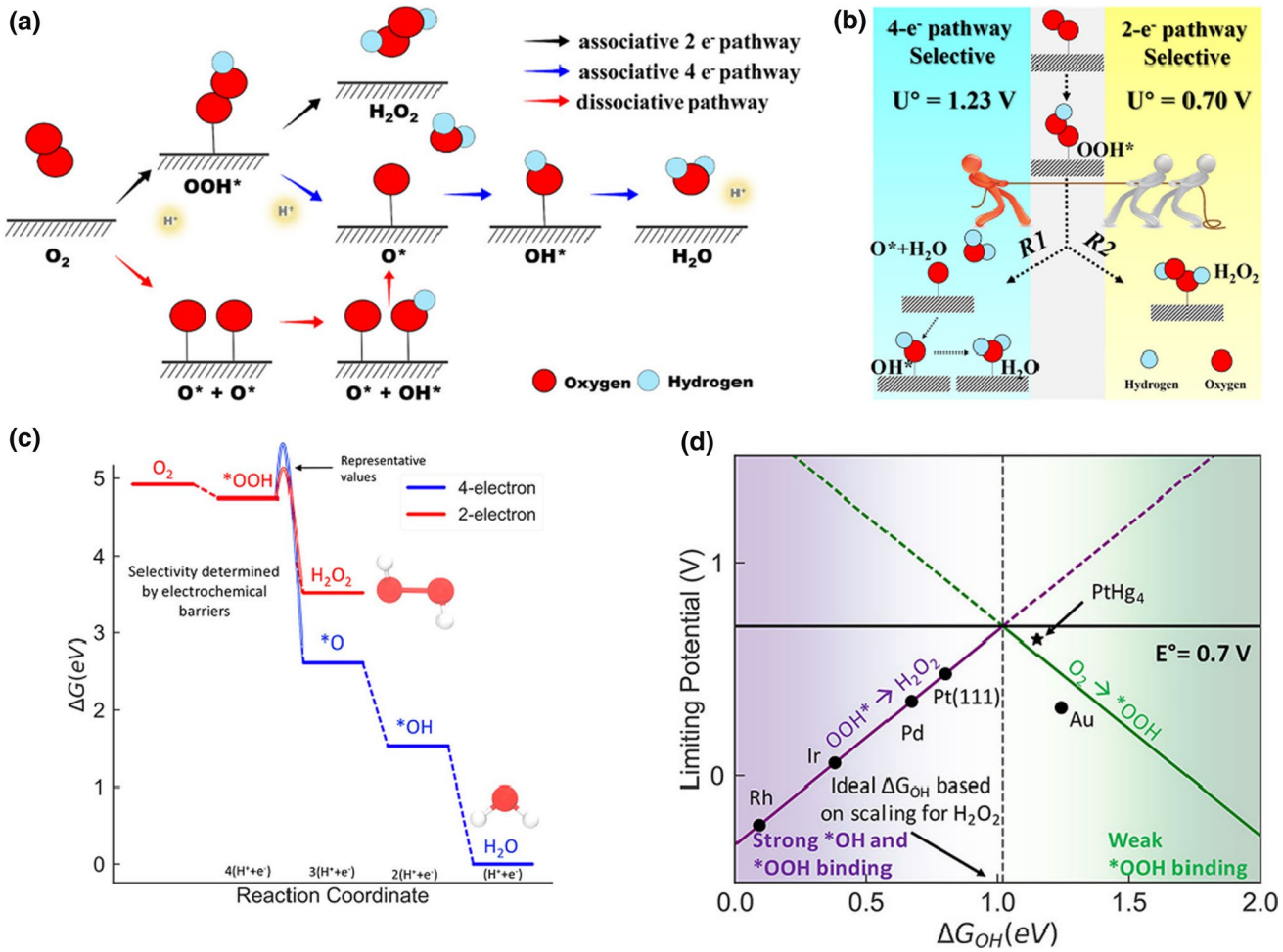

Fig. 1 **a** Three possible reaction pathways in electrochemical oxygen reduction reaction and **b** equilibrium potentials and the competition between two reaction pathways in associative electrochemical oxygen reduction reaction. Reprinted with permission of (Guo et al. 2019), *Copyright ACS*. **c** A free energy diagram of associative electrochemical oxygen reduction reaction via 2 e^- (red) and 4 e^- (blue) pathways and the energy barriers from *OOH to H_2O_2 or *O; **d** limiting potentials of individual reaction steps in Eq. (4) and Eq. (5), showing a strongly bound *OH region (solid purple line) and a weakly bound *OOH region (solid green line) for the 2 e^- pathway. Reprinted with permission of (Kulkarni et al. 2018), *Copyright ACS*

$$O_2 + 4\left(H^+ + e^-\right) \rightarrow 2H_2O \tag{8}$$

$$O_2 + * + * \rightarrow 2^*O \tag{9}$$

In the associate oxygen reduction reaction, there is a competition between H_2O_2 and H_2O formation from the *OOH reaction intermediate, as illustrated in Fig. 1b. The key to increasing the selectivity toward H_2O_2 (Eq. 3) is to suppress the dissociation of O–O bond in *OOH (Eq. (5)), which are controlled by the energy barriers of these two steps (Fig. 1c). Therefore, catalysts with strong O adsorption energies are unsuitable for H_2O_2 generation because they are more favorable for *O formation (Eq. 9). In contrast, catalysts with weaker O adsorption energies are more favorable for H_2O_2 generation (Lin et al. 2021; Wang et al. 2021b). However, many catalysts that show selectivity toward H_2O_2 formation are also catalytically active to further reduce H_2O_2 to H_2O because H_2O is the thermodynamically more stable final product for the oxygen reduction reaction.

Because *OOH is the only intermediate involved in the 2 e^- pathway toward H_2O_2 formation, the reaction limiting step would be forming or removing *OOH on a catalyst surface. The theoretical overpotential for H_2O_2 formation ($U_{H_2O_2}$) correlates with the adsorption energy of *OOH (ΔG_{HOO*}). Since the three possible reaction intermediates (*OOH, *O, and *OH) all bind to an active catalytic site through an O atom, their adsorption energies are correlated to each other by linear scaling relationships (Kulkarni et al. 2018). Thus, the adsorption energy of *OH (ΔG_{OH}) is often

used a descriptor in evaluating the catalytic activity of different oxygen reduction reaction catalysts. The limiting potentials for the two reactions (*OOH → H_2O_2 and O_2 → *OOH) can be expressed as Eq. 10 (green line in Fig. 1d) and Eq. 11 (purple line in Fig. 1d), respectively:

$$U_{*\mathrm{OOH}\rightarrow \mathrm{H_2O_2}} = -\Delta G_{\mathrm{HO}} + 1.72 \tag{10}$$

$$U_{\mathrm{O_2}\rightarrow *\mathrm{OOH}} = \Delta G_{\mathrm{HO}} - 0.32 \tag{11}$$

On the left side (solid purple line) of Fig. 1d, *OOH would adsorb strongly on a catalyst, and *OOH → H_2O_2 is the limiting step. The 4 e^- pathway to produce H_2O is favorable. In contrast, on the right hand (solid green line), *OOH would adsorb weakly on a catalyst, the selectivity toward H_2O_2 is high, but the catalytic activity would be negligible. Thus, an ideal catalyst with both high activity and selectivity toward H_2O_2 synthesis may be found at the peak in the middle, where the adsorption energy of *OOH on a catalyst is moderate.

Reactive oxygen species generation by H_2O_2 activation

The O–O bond strength in H_2O_2 (142 kJ mol^{-1}) is not strong; thus, it is relatively easy to cleave the O–O bond to generate ·OH. There is still no consensus on the detailed reaction mechanism of ·OH generation from H_2O_2. Two major reaction routes can generate ·OH from H_2O_2 in electro-Fenton processes: Fenton reactions or direct H_2O_2 reduction via a 1 e^- pathway. H_2O_2 is first generated on the cathode via electrochemical oxygen reduction reaction, as illustrated in Fig. 2a (Yang et al. 2018a). Conventional homogenous Fenton reactions occur by adding Fe^{2+} to the H_2O_2 solution at a low pH of around 3, yielding ·OH and Fe^{3+} (Eq. 12). It should be noted that when pH > 3, the formation of $Fe(OH)^+$ ions would result in a low activity in activating H_2O_2 to ·OH. Further, because ·OH has a short lifetime, Fe^{2+} needs to be added continuously to maintain a desirable ·OH concentration. For example, a previous study showed that 1 mM Fe^{2+} was needed for efficient perfluorooctanoate removal (Liu et al. 2015a). Although some Fe^{3+} may be directly reduced at the cathode to regenerate consumed Fe^{2+} (Eq. 13), significant $Fe(OH)_3$ sludge would be produced from Fe^{3+} as solid wastes. Alternatively, heterogeneous Fenton processes have been investigated to activate H_2O_2, in which Fe species are stabilized in solid catalysts and activate H_2O_2 to form surface bound radicals (Hou et al. 2017). Under neutral or even alkaline condition, surface-bound ·OH is formed via the reaction between surface Fe species (≡Fe(II)) and H_2O_2 (Eq. 14), contributing to pollutant degradation (Yu et al. 2019). A key advantage of heterogeneous Fenton processes is that it can be operated in a wider pH range than homogenous Fenton processes.

$$Fe^{2+} + H_2O_2 + H^+ \rightarrow {}^{\cdot}OH + H_2O + Fe^{3+} \tag{12}$$

$$Fe^{3+} + e^- \rightarrow Fe^{2+} \tag{13}$$

$$\equiv Fe(II) + H_2O_2 + H^+ \rightarrow \equiv Fe(III) + {}^{\cdot}OH + H_2O \tag{14}$$

In the other route, H_2O_2 generated on a cathode can be directly reduced to ·OH via the 1 e^- pathway and then desorb from the solid catalyst surface. The Gibbs free energy of generating ·OH from $*H_2O_2$ is -3.02 eV (Eqs. 15–16), which is much lower than that of the direct desorption of $*H_2O_2$ at -0.91 eV (Eq. (17); thus, the 1 e^- pathway is thermodynamically favorable. The overall reaction from O_2 to ·OH can be considered as an electrochemical oxygen reduction reaction via a 3 e^- pathway (Eq. 18), as illustrated in Fig. 2b (Xiao et al. 2021a).

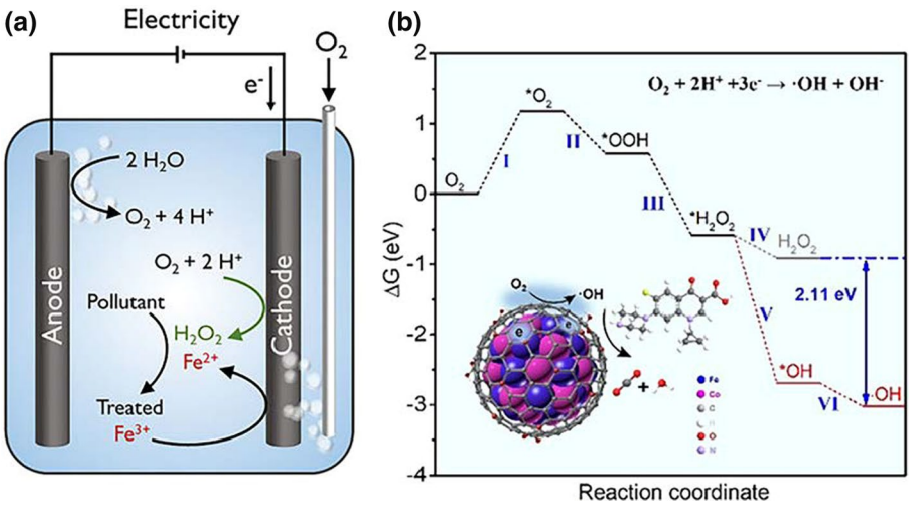

Fig. 2 **a** Generation of H_2O_2 on the cathode and activation of H_2O_2 in an electro-Fenton process. Reprinted with permission of (Yang et al. 2018a), *Copyright ACS*. **b** A free energy diagram of ·OH generation from O_2 by electrochemical oxygen reduction reaction via a 3e^- pathway on a FeCo alloy catalyst encapsulated by carbon aerogel. Reprinted with permission of (Xiao et al. 2021a), *Copyright Wiley*

$$* H_2O_2 + e^- \rightarrow * OH + OH^- \quad (15)$$

$$* OH \rightarrow * + {}^{\cdot}OH \quad (16)$$

$$* H_2O_2 \rightarrow * + H_2O_2 \quad (17)$$

$$O_2 + 2H^+ + 3e^- \rightarrow {}^{\cdot}OH + OH^- \quad (18)$$

In addition to the major reactive oxygen species ($^{\cdot}OH$) in the Fenton process, several other types of reactive oxygen species may also be generated via H_2O_2 activation. Hydroperoxyl radicals ($HO_2^{\cdot}$) with a lower oxidation power can also be produced ($H_2O_2 + OH^- \rightarrow H_2O + HO_2^{\cdot}$) (Tang and Wang 2018). $HO_2^{\cdot}$ may react with H_2O_2 to generate $HO^{\cdot}$ ($HO_2^{\cdot} + H_2O_2 \rightarrow HO^{\cdot} + H_2O + O_2$). Alternatively, $HO_2^{\cdot}$ can react with $^{\cdot}OH$ to form O_2. $HO_2^{\cdot}$ can also facilitate the reduction of Fe(III) to Fe(II) ($Fe(III) + HO_2^{\cdot} \rightarrow Fe(II) + H^+ + O_2$). Further, Fe(IV) has also been identified as reactive oxygen species in the Fenton process ($Fe(II) + H_2O_2 \rightarrow H_2O + Fe(IV)O^{2+}$) (Wang and Wang 2020).

Bifunctional catalysts for reactive oxygen species generation from O_2

The above reaction mechanisms indicate that an efficient catalyst is essential for H_2O_2 synthesis via electrochemical oxygen reduction reaction and the activation of H_2O_2 to generate $^{\cdot}OH$ in heterogeneous electro-Fenton processes (Wang et al. 2013; Liu et al. 2018; Su et al. 2019). Traditionally, two different catalysts are required for these two steps separately. Recent studies show that some Fe or alloys nanoparticles encapsulated in carbon substrates have excellent activities for both $2e^-$ oxygen reduction reaction and heterogenous Fenton reactions, which may serve as bifunctional catalysts for reactive oxygen species generation directly from O_2. Further, some transition metal single-atom catalysts and metal-free carbon catalysts also show promising catalytic activities as bifunctional catalysts. We will discuss recent advances in these new catalysts in the following subsections, respectively. Their electrocatalytic performance for contaminant degradation is summarized in Table 1.

Metal/carbon composite catalysts

Monometallic Fe/carbon composite catalysts

Iron species supported on a wide range of materials have been used as catalysts for heterogeneous Fenton processes (Munoz et al. 2015). Carbon materials, such as activated carbon, carbon nanotubes, and graphene, provide high specific surface area, porous structures, and relatively good chemical stability. They are often used as substrates of Fe catalysts in heterogeneous Fenton processes. Efficient electron transfer is important for electro-Fenton processes. Carbon materials with their conductive matrix can provide efficient electron transfer. Thus, they are widely used as conductive substrates for electrocatalysts. Recent studies have shown that oxidized carbon materials are also efficient catalysts for H_2O_2 generation by the $2e^-$ ORR (Lu et al. 2018). Thus, Fe catalysts supported on carbon materials are promising bifunctional catalysts, in which carbon materials catalyze the synthesis of H_2O_2 and Fe species activate H_2O_2 to generate ROS.

For example, Gao et al. (2015) chelated Fe^{2+} with partially oxidized carbon nanotubes via surface carboxylate groups, which were used as a bifunctional catalyst to synthesize and active H_2O_2 to $^{\cdot}OH$. However, due to relatively weak electrostatic interactions between oxidized carbon nanotubes and Fe^{2+}, significant Fe^{2+} was leached during reactions. As shown in Fig. 3a, about 95% H_2O_2 was activated in 5 min in the first reaction cycle, whereas only around 5% H_2O_2 was activated in 5 min in the second cycle. The leaching of Fe^{2+} led to fast catalyst deactivation. In another study, Yao et al. (2021) synthesized $Fe^{II}Fe^{III}$ layered double hydroxide on carbon felt as a bifunctional catalyst. Similarly, Fe^{2+} leached easily from catalysts in acidic solutions.

Forming strong chemical bonds between Fe species and carbon substrates or trapping Fe species inside carbon structures have been explored to reduce Fe leaching, thus improving catalyst stability and reusability. For example, Wang et al. (2013) incorporated 5 wt.% ferrites (Fe_2O_3) into a 3D carbon aerogel. The carbon aerogel itself did not catalyze the decomposition of H_2O_2. At low pH, both dissolved Fe ions and surface Fe contributed to the activation of H_2O_2. At neutral pH, surface Fe species activate H_2O_2. Liu et al. (2018) fixed highly dispersed Fe_3O_4 nanoparticles on carbon nanofibers (CNFs) via covalent bonds. The H_2O_2 was generated in situ on CNFs, then was activated to $^{\cdot}OH$ on Fe_3O_4 nanoparticles. This bifunctional catalyst can effectively degrade carbamazepine and retain 90% of its catalytic activity after 3 reaction cycles. However, only the surface of nonporous Fe_3O_4 nanoparticles could contribute to $^{\cdot}OH$ generation. Increasing the mass loading of Fe_3O_4 nanoparticles on CNFs would result in Fe_3O_4 nanoparticle aggregation, limiting the specific activity of this catalyst. Wang et al. (2021c) synthesized carbon nanotubes from Fe/Fe_3C nanoparticles loaded on carbonized wood. The composite materials were used as self-supported cathode and anode. Fe/Fe_3C nanoparticles and carbon nanotubes acted as a bifunctional catalyst.

Metal–organic frameworks are porous materials consisting of metal ions or clusters coordinated to organic ligands. Because their large specific surface and porous structures can host abundant and easily accessible metal catalytic active sites after carbonization, they have been

Table 1 Catalytic performance comparison of recently reported bifunctional electrocatalysts used in heterogeneous electro-Fenton processes

	Catalysts	Pollutants	Initial Conc. (mg/L)	Operation condition		Performance		Roles of bifunctional catalysts		Notes	References
				Potential/Current	Electrolyte pH	Time (min)	Removal efficiency	H_2O_2 generation	H_2O_2 activation		
Monometallic Fe/carbon composite catalysts	$Fe^{II}Fe^{III}$ LDH[a] on carbon felt	Ciprofloxacin	66.3	200 mA	6	90	88.11%	Carbon felt	$Fe^{II}Fe^{III}$ LDH	Anode: Ti/RuO_2-IrO_2; Both homogeneous and heterogeneous process	Yao et al. (2021)
	Fe@Fe_2O_3/ carbon aerogel	Metalaxyl	500	10 mA cm^{-2}	6	240	98%	Carbon aerogel	Surface Fe	Anode: BDD[b] Mainly heterogeneous process	Wang et al. (2013)
	Fe_3O_4/graphite felt	Levofloxacin	80	1 mA/cm^2	6.75	100	72.5%	Graphite felt	Fe_3O_4		Huang et al. (2022)
	Fe_3O_4 CNF[c]	Carbamazepine	1.0	−0.345 V versus RHE[l]	7	30	100%	CNF	Fe(II)		Liu et al. (2018)
	Fe/Fe_3C/CNT[d]	As(III)	1.0	−0.2 V versus Ag/AgCl	6	90	99%	CNT	Fe_3C or Fe clusters	Anode and cathode are both self-standing	Wang et al. (2021c)
	CMIL-100@PCM[e]	Napropamide	10	−0.14 V versus RHE	7	60	82.3%	PCM	Fe_3O_4		Liu et al. (2019)
	CMIL-88-NH_2@PCM	Napropamide	10	−0.14 V versus RHE	7	60	73.4%	PCM	Fe_3C and Fe_3O_4		Liu et al. (2019)
	MIL-101(Fe)- carbon felt	p-nitrophenol	50	10 mA	3	120	100%	Fe–O sites; carbon layer	Fe_3O_4		Dong et al. (2021)
	MIL-101(Fe)-CNT	Tetracycline	0.04 mM	−2 V	6.5	120	93.2%	O-CNT	Fe(II)		Dai et al. (2022)
	FeO_x/NHPC[f]	Phenol	50	−0.6 V versus RHE	6	120	99%	Pyridinic and pyrrolic N	FeO_x; graphitic N		Cao et al. (2020a)
	FeNC@C	Chlorophenol	0.2 mM	−0.6 V versus RHE	3	30	90%	Fe_3C	FeN_x		Hu et al. (2021c)
					9	60	60%				
	Fe_3N@NG/NC[g] on carbon felt	Rhodamine B	10	0.0 V versus RHE	5	60	96%	Carbon felt, Fe_3N, pyridinic N	Fe_3N; graphitic N		Xiao et al. (2021b)
	rGO[h]@Fe_xP/C	Sulfamethoxazole	10	−0.45 V versus SCE[m]	6	45	100%	rGO	Fe(II)	rGO layer could significantly prevent Fe_xP from dissolving	Cheng et al. (2021), Huang et al. (2022)
	H_2O_2 synthesis is catalyzed by carbon, while Fe species activate H_2O_2 to form ·OH. They often can work in a wide range of pH (e.g., 3 to 9). Some catalysts display good stability with negligible leaching of Fe ions. N doping may promote the recycling of Fe(II)										
Bimetallic or trimetallic/carbon composite catalysts	FeCo/Carbon felt	Tetrabromobisphenol A	10	−0.6 V versus SCE	3	60	95%	Carbon felt	FeCo MOFs		Wang et al. (2022b)

Table 1 (continued)

Catalysts	Pollutants	Initial Conc. (mg/L)	Operation condition		Performance		Roles of bifunctional catalysts		Notes	References
			Potential/Current	Electrolyte pH	Time (min)	Removal efficiency	H_2O_2 generation	H_2O_2 activation		
FeCo@ordered mesoporous carbon	Rhodamine B	5	− 1.3 V versus SCE	7	120	99%	Ordered mesoporous carbon	FeCo alloy	Confined space in mesoporous carbon to restrict the size of alloy nanoparticles and interconnected channels for improved mass transfer	Chen et al. (2022)
$CoFe_2O_4$/ Carbon felt	Tartrazine	50	8.33 mA/cm^2	3	40	97.05%	Carbon felt	Surface Fe(II) and Co(II)		Dung et al. (2022)
FeCo/nitrogen-doped porous carbon rods	Tetracycline	20	100 mA	7	60	91%	N-doped porous carbon	Surface Fe(II) and Co(II)		Hu et al. (2021d)
Cu–Fe/Fe_3C@carbon felt	Methylene blue		− 1.1 V versus RHE	3	30	99.9%	Fe_3C, carbon felt	Surface Fe(II) and Cu(I)		Yang et al. (2022)
FeCuC aerogel	Methylene blue	50	20 mA	7	30	98%	CA	Surface Fe(II) and Cu(I)	Anode: BDD; Cu^0 served as a reduction promoter	Zhao et al. (2016a)
FeCuC aerogel	Dimethyl phthalate	50	30 mA	7	60	85%	Fe@Fe_3C; Cu^0; CA	Surface Fe(II) and Cu(I)	Anode: BDD;	Zhao et al. (2018)
Mn/Fe@PC^i + carbon black	Triclosan	10	40 mA	3	120	100%	Mn/Fe@PC; carbon black	Surface Fe(II) and Mn(II/III)	Direct regeneration of Fe(II) and Mn(II/III) promoting H_2O_2 utilization	Zhou et al. (2020)
Ce/Fe-graphite felt	Sulfamethoxazole	20	20 mA	3	120	100%	Graphite felt	Surface Fe(II) and Ce(III)	Synergistic effect of Fe–Ce promoting the regeneration of Fe(II)/Ce(III)	Qiu et al. (2021)

Table 1 (continued)

	Catalysts	Pollutants	Initial Conc. (mg/L)	Operation condition		Performance		Roles of bifunctional catalysts		Notes	References
				Potential/Current	Electrolyte pH	Time (min)	Removal efficiency	H_2O_2 generation	H_2O_2 activation		
	Ce/α-FeOOH on Carbon felt	Chloramphenicol	355	30 mA	3	8 h	100%	Carbon felt	Surface Fe(II) and Ce(III)		Liu et al. (2021b)
	Fe/Mo-graphite felt	Ciprofloxacin	10	− 0.6 V versus Ag/AgCl	6	90	100%	Graphite felt	Surface Fe(II)	Anode: RuO_2/Ti mesh Mo(IV) promoting the conversion of Fe (III)/Fe (II)	Liu et al. (2021d)
	$NiMn_2O_4$-Carbon felt	Ciprofloxacin	30	–	3	90	100%	Carbon felt	Surface Mn(III) and Ni(II)		Sun et al. (2019)
	$LaCo_xCu_{1-x}O_{3-\delta}$ on carbon felt	Ciprofloxacin	20	75 mA	3	120	98.8%	Carbon felt	Surface Co(II) and Cu(I); Oxygen vacancies		Xie et al. (2022)
	FeCo alloy in carbon aerogel	Ciprofloxacin	10	24 mA	3	5	100%	Carbon aerogel	$1e^-$ pathway		Xiao et al. (2021a)
	CoFe LDHs on Carbon felt	Acid orange II	40	38 mA	3	10	100%	Carbon felt	CoFe–LDH	Both homogeneous and heterogeneous EF process	Ganiyu et al. (2017)
	CoFe-LDH/Carbon felt	Norfloxacin	0.1 mM	50 mA	6	30	100%	Carbon felt	CoFe–LDH	Anode: BDD;	Yu et al. (2021a)
	The additional metals, such as Ce, Co, and Mn, may also activate H_2O_2 to generate $^{\cdot}OH$. They may form redox couples to facilitate the reduction of Fe(III) to Fe(II). Cu may create oxygen vacancy, reducing adsorbed O_2 to generate $\cdot O_2^-$. The local electronic environment of carbon may be tuned by electrons from encapsulated alloy nanoparticles, resulting in the activation of H_2O_2 to $\cdot OH$ by the $1\ e^-$ pathway										
Single-atom catalysts	Iron anchored on PC	Sulfamethoxazole	30	0.15 V versus RHE	6	60	100%	PC	Single iron species	Selective oxidation by probe molecules	Cao et al. (2020b)
	Fe/N-DG[j]	Chloramphenicol	25	0.6 V versus RHE	13	180	97.6%	Pyridinic-N and oxygen defects	Atomically dispersed Fe species		Song et al. (2021)
	Fe@HSC[k]	Thiamphenicol	20	60 mA	7	40	100%	Fe atoms; carbon	Fe atoms		Zhang et al. (2022a)
	FeCuSA-NPC	4-chlorophenol	20	− 0.6 V versus SCE	5	60	95%	Carbon	Fe–N	Cu–N sites adsorbing 4-chlorophenol	Zhao et al. (2021)
	Atomically dispersed metal atoms serve as active sites. Extra function groups may be introduced near active sites to achieve selective degradation of organics, such as chlorinated organics										

Table 1 (continued)

	Catalysts	Pollutants	Initial Conc. (mg/L)	Operation condition		Performance		Roles of bifunctional catalysts		Notes	References
				Potential/Current	Electrolyte pH	Time (min)	Removal efficiency	H_2O_2 generation	H_2O_2 activation		
Metal composite catalysts without carbon	$CuCo_{2-x}Ni_xS_4$	Rhodamine B	20	0.25 V versus RHE	1.2	150	40%	$CuCo_{2-x}Ni_xS_4$	Cu^+	Homogeneous EF process	Ross et al. (2021)
	Ti^{3+}/TiO_2 nanotube arrays	phenol	20	−0.8 V	3–9	45	100%	Ti^{3+}/TiO_2	Ti^{3+}/TiO_2	H_2O_2 reduced to •OH in situ without desorption by 1 e^- electrocatalytic reduction	Wang et al. (2022a), Zhang et al. (2022b)
	There are few studies in this area so far. Synthesis and activation of H_2O_2 may occur on the same or different metal active sites in metal composite catalysts. Metal composition and their ratios strongly influence their catalytic activity										
Metal-free carbonous catalysts	Oxidized CNTs	Phenol	20	−0.4 V versus SCE	6.5	60	99.2%	sp^3-C	-C = O group		Qin et al. (2021)
	PCMs	Napropamide	10	−0.146 V versus RHE	7	60	80%	-C = O group and sp^3-C	1 e^- pathway		Yu et al. (2021b)
	N-doped graphene	Phenol	25	−1.1 V versus Ag/AgCl	7	120	100%	Graphite N	Pyridinic N	Anode: DSA	Su et al. (2019)
	GF with N-doped graphene	Phenol	50	−0.9 V	7	50	97%				Yang et al. (2018b)
	GF with N-doped graphene	2,4-Dichlorophenoxiacetic acid	20	4 V	7	20	100%	Graphite N	Pyridinic N		Su et al. (2019), Yang et al. (2019)
	B-doped graphene	Bisphenol A	10	2.7 mA	3	60	100%	Electrophilic B sites	$-BC_3$		Wu et al. (2019)
	Boride activated carbon	Phenol	30	−0.2 V versus RHE	3	30	99%	$-BC_3$, $-BC_2O$ groups	$-BC_3$, $-BC_2O$		Chen et al. (2021)
	Introducing heteroatom atoms disrupts the electronic structures of sp^2-hybridized carbon materials and creates active sites for H_2O_2 synthesis and activation. Many works have studied their activities for the 2e^- oxygen reduction reaction; however, few studies have investigated their bifunctional activities										

[a]LDH—layered double hydroxide; [b]BDD—boron-doped diamond; [c]CNF—carbon nanofiber; [d]CNT—carbon nanotube; [e]PCM—porous carbon monolith; [f]NHPC—N-doped hierarchically porous carbon; [g]Fe_3N@NG/NC—N-doped carbon-coated iron nitride composite; [h]rGO—reduced graphene oxide; [i]Mn/Fe@PC—Fe, Mn-doped porous carbon; [j]DG—defect-enriched graphene sheets; [k]HSC—hollow sea-urchin-shaped carbon; [l]RHE—reversible hydrogen electrode; [m]SCE—saturated calomel electrode

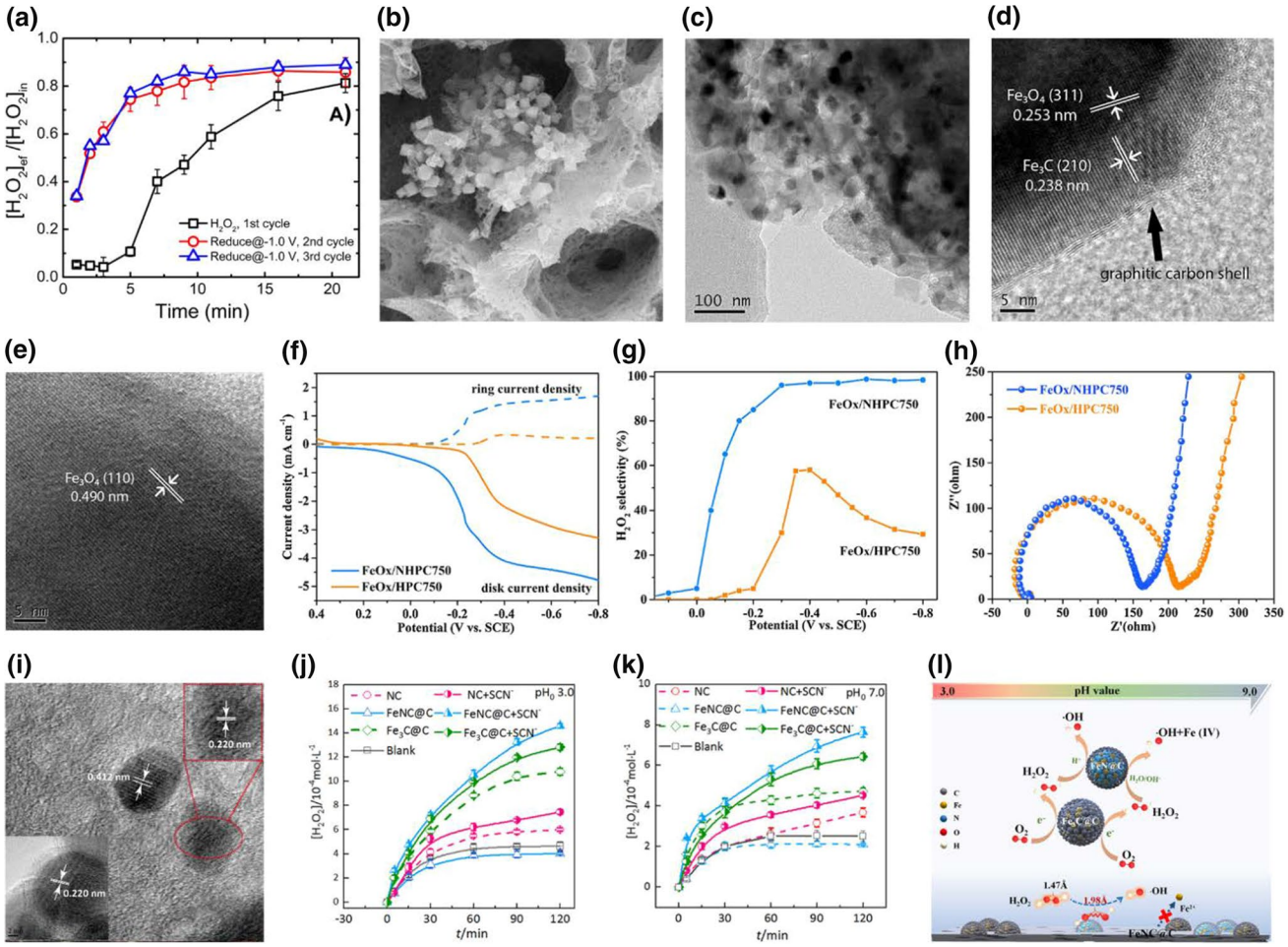

Fig. 3 **a** Activation of H_2O_2 on a heterogenous electro-Fenton reaction catalyst (carbon nanotube-COOFe^{2+}) and its regeneration by reduction over 3 reaction cycles. $[H_2O_2]_{ef}$ and $[H_2O_2]_{in}$ refer to the concentration of H_2O_2 in effluent and influent of the flow-through electro-Fenton reactor, respectively. Reprinted with permission of (Gao et al. 2015), *Copyright ACS*. **b** A scanning electron microscopy (SEM) image and **c** a transmission electron microscopy image of metal–organic framework nanoparticles anchored inside macropores of carbon monolith, **d** a transmission electron microscopy image of a core–shell nanoparticle derived from MIL-88-NH_2 metal–organic framework, showing a core–shell structure, **e** a transmission electron microscopy image of a Fe_3O_4 nanoparticle derived from a metal–organic framework (MIL-88). Reprinted with permission of (Liu et al. 2019), *Copyright ACS*. **f** Polarization curves of FeO_x/NHPC750 and FeO_x/HPC750 catalysts at 1200 rpm (solid lines) with a scan rate of 10 mV s^{-1} and simultaneous H_2O_2 oxidation currents at the ring electrode (dashed lines), N doping improving the selectivity and activity for 2e$^-$ oxygen reduction reaction **g** the corresponding H_2O_2 selectivity related to (**f**), (**h**) electrochemical impedance spectroscopy curves of FeO_x/NHPC750 and FeO_x/HPC750 catalysts obtained in an Ar-saturated electrolyte, a lower charge transfer resistance of FeO_x/NHPC750 than FeO_x/HPC750. Reprinted with permission of (Cao et al. 2020a), *Copyright Elsevier*. **i** A transmission electron microscopy image of FeNC@C catalyst, with Fe_3C and FeN_x nanoparticles uniformly distributing in graphitic layers, **j**–**k** H_2O_2 synthesis in electrolytes with and without SCN$^-$ at pH 3 and pH 7, respectively, and **l** Fe_3C acting as active sites for H_2O_2 synthesis, and H_2O_2 activation on FeN_x nanoparticles in heterogenous electro-Fenton reaction. Reprinted with permission of (Hu et al. 2021c), *Copyright ACS*

used as precursors to synthesize bifunctional catalysts (Cheng et al. 2018). For example, Liu et al. (2019) reported a bifunctional catalyst by anchoring calcinated Fe containing Metal–organic framework nanoparticles on porous carbon monolithic substrates. Calcinated metal–organic frameworks nanoparticles uniformly deposited in macropores of carbon monolith are easily accessible by electrolytes and dissolved O_2 molecules (Fig. 3b, c). The porous carbon monolith can catalyze H_2O_2 synthesis over a wide pH range (4, 7, and 10) with a much higher production rate than nonporous carbon materials. The close interactions between calcinated metal–organic framework nanoparticles and active catalytic sites in carbon monolith also enabled much faster ·OH generation. The resulting catalytic activity depended on the specific metal–organic framework precursor used (MIL-88-NH_2). The MIL-88-NH_2 derived nanoparticles show a core–shell structure, in which a Fe_3C intermediate layer is sandwiched

between a graphitic carbon shell and a Fe_3O_4 core (Fig. 3d). Despite their similar specific surface area and pore structures, they delivered a higher reaction rate constant, almost twice those derived from the metal–organic framework (MIL-88) without the Fe_3C intermediate layer (Fig. 3e) (Liu et al. 2019). It was proposed that the Fe_3C intermediate layer acted as quasi electron conductors, which facilitate the electron transfer between the Fe_3O_4 core and graphitic carbon shells. The Fe_3C intermediate layer also helped to lock Fe in Fe_3O_4 and Fe_3C, inhibiting the leaching of Fe^{2+}. Thus, the catalyst had no significant changes in its degradation performance after 3 reaction cycles. In a recent study, Dong et al. (2021) pyrolyzed a metal–organic framework (MIL-101(Fe)) anchored on a polyaniline-modified carbon fiber paper at 400 ℃. The resulting catalyst contained Fe_3O_4 nanoparticles covered by graphene-like carbon layers. The catalyst retained good performance after 10 reaction cycles.

The slow in situ H_2O_2 synthesis and inefficient surface Fe(II) regeneration are often the bottlenecks of Fe/C composite catalysts. Incorporating N into Fe/C composite catalysts has shown promising results in resolving these bottlenecks. For example, Cao et al. (2020a) embedded FeO_x nanoparticles derived from a metal–organic framework (NH_2-MIL-88B(Fe)) into N-doped hierarchically porous carbon (FeO_x/NHPC750). Doped N atoms, especially pyridinic and pyrrolic N, modified the electronic structures of carbon materials to optimize the adsorption of *OOH intermediate, which improved the selectivity and activity for $2e^-$ oxygen reduction reaction. FeO_x/NHPC750 showed an overpotential (~ 190 mV) in H_2O_2 synthesis much lower than that of FeO_x/HPC750 without N doping (~ 390 mV) (Fig. 3f) and higher selectivity (95–98%) (Fig. 3g). Further, graphitic N atoms with higher electronegativity can extract electrons from adjacent C atoms. The resulting positively charged carbon substrates facilitate electron transfers with FeO_x nanoparticles, enhancing the regeneration of surface Fe(III) to Fe(II). Figure 3h shows that FeO_x/NHPC750 has a lower charge transfer resistance than FeO_x/HPC750. Hu et al. (2021c) synthesized a core–shell structured Fe catalyst (FeNC@C) containing Fe_3C and FeN_x nanoparticles encapsulated by porous graphitic layers. Figure 3i shows that Fe_3C and FeN_x nanoparticles distribute uniformly in graphitic layers. The comparison of H_2O_2 synthesis with or without FeN_x sites blocked by SCN^- at pH 3 (Fig. 3j) and 7 (Fig. 3k) suggested that Fe_3C served as active sites for H_2O_2 synthesis while FeN_x were H_2O_2 activation active sites (Fig. 3l). Density functional theory calculation results show that Fe atoms on FeN_x have a higher H_2O_2 binding energy than that on Fe_3C, which could elongate the O–O bond length of absorbed H_2O_2 from 1.47 to 1.98 Å, beneficial for $^{\cdot}OH$ formation. Xiao et al. (2021b) carried out simultaneous carbonization and NH_3 etching of Fe-metal–organic framework materials, yielding homogeneously dispersed Fe_3N nanoparticles (70 nm) in an N-doped graphitic carbon framework. The Fe_3N nanoparticles and pyridinic N promoted the H_2O_2 activation to generate $^{\cdot}OH$ with low leaching over 6 reaction cycles.

Bimetallic or trimetallic carbon composite catalysts

Bimetallic or trimetallic catalysts, which combine metal species with variable valences, such as Fe, Cu, Co, Ce, Mn, Mo, Ni, and La, have demonstrated high activity and stability as bifunctional catalysts. Several synthesis routes have been reported to obtain bimetallic or trimetallic catalysts (Yan et al. 2021; Wang et al. 2022b; Yang et al. 2022). The most common approach is incorporating metal alloy nanoparticles or multi-metal composites in carbon substrates. For example, Zhao et al. (2016a) used metal-resin precursors containing Fe and Cu to synthesize a porous bimetallic catalyst (FeCuC aerogel). A two-step gas activation process was applied. The calcination in CO_2 first increased the accessibility of metal sites in carbon aerogel. Next, the calcination in N_2 further increased porosity and reduced metal oxides to Fe^0 and Cu^0. The porous carbon aerogel catalyzed H_2O_2 synthesis via $2e^-$ oxygen reduction reaction at a wide pH range (3–9). Surface Fe(II) activated H_2O_2 to create $^{\cdot}OH$ (Eq. 14). The regeneration of Fe(II) from Fe(III) occurred directly on catalyst surfaces under the applied potential on the cathode (Eq. 19). The authors proposed that Cu^0 served as a reduction promoter to enhance electron transfer. Further, the surface Cu(I)/Cu(II) cycle (Eq. 20) also activated H_2O_2 to create $^{\cdot}OH$ (Eq. 21). Importantly, negligible Fe and Cu leaching was observed even in acidic solutions due to the efficient encapsulation of Fe and Cu species in the porous carbon aerogel. Another Fe-Cu embedded carbon aerogel was reported as a bifunctional catalyst. It was proposed that Fe/Fe_3C encapsulated by graphitic layers would boost oxygen reduction reaction activity, while Cu's existence improved the selectivity toward H_2O_2 generation. The catalyst showed high degradation efficiency after 6 reaction cycles (Zhao et al. 2018).

$$\equiv \mathrm{Fe(III)} + e^- \rightarrow \equiv \mathrm{Fe(II)} \tag{19}$$

$$\equiv \mathrm{Cu(II)} + e^- \rightarrow \equiv \mathrm{Cu(I)} \tag{20}$$

$$\equiv \mathrm{Cu(I)} + H_2O_2 + H^+ \rightarrow \equiv \mathrm{Cu(II)} + {}^{\cdot}OH + H_2O \tag{21}$$

Several other combinations of different metal species have been explored. For example, Mn and Fe were incorporated into porous carbon by carbonizing Mn-doped MIL-53(Fe) metal–organic framework. The electron transfer between surface Fe(II)/Fe(III) and Mn(II)/Mn(III)/Mn(IV) promoted the activation of H_2O_2 (Zhou et al. 2020). Ce and

Fe were loaded on graphite felt. The authors proposed that the introduction of CeO_2 improved the chemical absorption of O_2, thus boosting the generation of H_2O_2. The coexistence of surface Fe(II)/Fe(III) and Ce(III)/Ce(IV) redox couples enhanced interfacial electron transfer, which promoted H_2O_2 synthesis and activation (Qiu et al. 2021). Liu et al. (2021d) synthesized FeOCl and MoS_2 on graphite felt. The authors proposed that the electron transfer between surface Fe(II)/Fe(III) and Mo(IV)/Mo(VI) boosted H_2O_2 synthesis and activation. Sun et al. (2019) synthesized mesoporous $NiMn_2O_4$ nanoparticles on carbon felt. The two redox couples (Mn(IV)/Mn(III) and Ni(III)/Ni(II)) increased the generation of radicals.

Alternatively, Xie et al. (2022) loaded $LaCoO_3$ perovskite incorporated with Cu ($LaCo_xCu_{1-x}O_{3-\delta}$) on oxidized carbon felt. They found that H_2O_2 synthesis catalyzed by carbon felt declined after loading $LaCo_xCu_{1-x}O_{3-\delta}$. However, the overall efficiency in producing $^{\cdot}OH$ increased significantly. The redox pairs (Co(II)/Co(III) and Cu(I)/Cu(II)) played similar roles as other bimetallic catalysts in facilitating the generation of radicals. Further, the authors proposed introducing Cu in $LaCoO_3$ could form more oxygen vacancies. Oxygen vacancies could facilitate the formation of adsorbed O species and efficiently promote the generation of $^{\cdot}OH$ from H_2O_2. Moreover, the interaction between oxygen vacancies and O_2 could also reduce adsorbed O_2 to generate $^{\cdot}O_2^-$ (Eq. 22), which is also an efficient reactive oxygen species for contaminant degradation.

$$O_2 + e^- \rightarrow \cdot O_2^- \tag{22}$$

A recent study proposed another reaction mechanism for FeCo alloy nanoparticles encapsulated in carbon aerogel (Xiao et al. 2021a). Rather than activating H_2O_2 by surface metal species, Xiao et al. (2021a) proposed that the carbon shell would activate H_2O_2 to $^{\cdot}OH$ by the 1 e^- pathway, whose local electronic environment was tuned with electrons from encapsulated FeCo alloy nanoparticles. The new approach of $^{\cdot}OH$ generation avoided the slow surface Fe(II)/Fe(III) regeneration and demonstrated excellent stability over 50 reaction cycles.

A unique approach to synthesize bimetallic catalysts transition is to anchor metal-based layered double hydroxides on carbon substrates. Layered double hydroxides are ionic solids with a layered structure that contain metallic cations octahedrally coordinated by hydroxyl groups. They can provide well-dispersed metal sites. Ganiyu et al. (2017) synthesized CoFe layered double hydroxides on carbon felt. Some Fe^{2+}/Co^{2+} leached from the catalyst joined homogeneous Fenton reactions in low pH acidic solutions. At neutral pH, surface-catalyzed reaction demonstrated good stability over 7 reaction cycles. In a recent study, Yu et al. (2021a) synthesized CoFe layered double hydroxides supported on carbon felts (CoFe-LDH/CF) by a hydrothermal process at temperatures ranging from 70 to 150 °C. The synthesis temperature strongly influenced catalyst morphology, specific surface area, and active catalytic sites. Figure 4a compares the catalytic performance of CoFe-LDH/CF synthesized at different temperatures in norfloxacin removal (quantified by total organic carbon) at different pH (3, 6, and 9). CoFe-LDH/CF synthesized at high temperatures (120 and 150 °C) only showed high activity in acidic solutions, which was attributed to homogenous Fenton reactions catalyzed by Fe^{2+} and Co^{2+} leached from the catalyst (Eq. 12 and Eq. 23). In contrast, CoFe-LDH/CF synthesized at lower temperatures (70 and 90 °C) showed better performance at pH 6 and 9. Density functional theory calculations were performed to understand the reaction mechanisms. Figure 4b shows that the reduction of *OOH to H_2O_2 has a lower barrier (-0.417 eV) on carbon surfaces, while the high O_2 adsorption energy on CoFe-LDH indicates that active catalytic sites for H_2O_2 synthesis are on carbon felts. Further, Fig. 4c shows that the energy required for the reaction step from *OOH to H_2O_2 changes from downhill at pH = 0 or 3 to uphill at pH = 6, 9, or 11, explaining a decrease in H_2O_2 synthesis in neutral or basic solutions. Density functional theory calculations also examined the H_2O_2 reduction pathway via the 1 e^- transfer to generate $^{\cdot}OH$ on CoFe-LDH (Fig. 4d) and the competitive H_2O_2 oxidation pathway to O_2 (Fig. 4e). H_2O_2 synthesized on carbon felts would first desorb from carbon felts and then be adsorbed on Co or Fe sites (Eq. 24) in both pathways. In the reduction pathway, $*H_2O_2$ receives 1 e^- to become *OH intermediate (Eq. 15). In contrast, $*H_2O_2$ loses 1 e^- to become *OOH in the oxidation pathway. The density functional theory calculation results showed that the desorption of $^{\cdot}OH$ (Eq. 16) from a Co atom (2.61 eV) or a Fe atom (3.44 eV) both have high energy barriers, indicating that $^{\cdot}OH$ generation on Co and Fe sites is unfavorable. Based on the density functional theory calculation results in this study, it is still challenging to explain the fast $^{\cdot}OH$ generation on CoFe-LDH/CF unless organic contaminate molecules could strongly bond to surface bonded $^{\cdot}OH$, as illustrated in Fig. 4f. On the other hand, the beneficial roles of Co could come from two aspects: leached Co^{2+} might contribute to the regeneration of Fe^{3+} (Eq. 25), and Co sites might be more favorable than Fe sites for $^{\cdot}OH$ generation.

$$Co^{2+} + H_2O_2 \rightarrow Co^{3+} + OH^- + \cdot OH \tag{23}$$

$$* + H_2O_2 \rightarrow * H_2O_2 \tag{24}$$

$$Fe^{3+} + Co^{2+} \rightarrow Fe^{2+} + Co^{3+} \tag{25}$$

In summary, compared to monometallic Fe/carbon composite catalysts, additional metals in bimetallic or

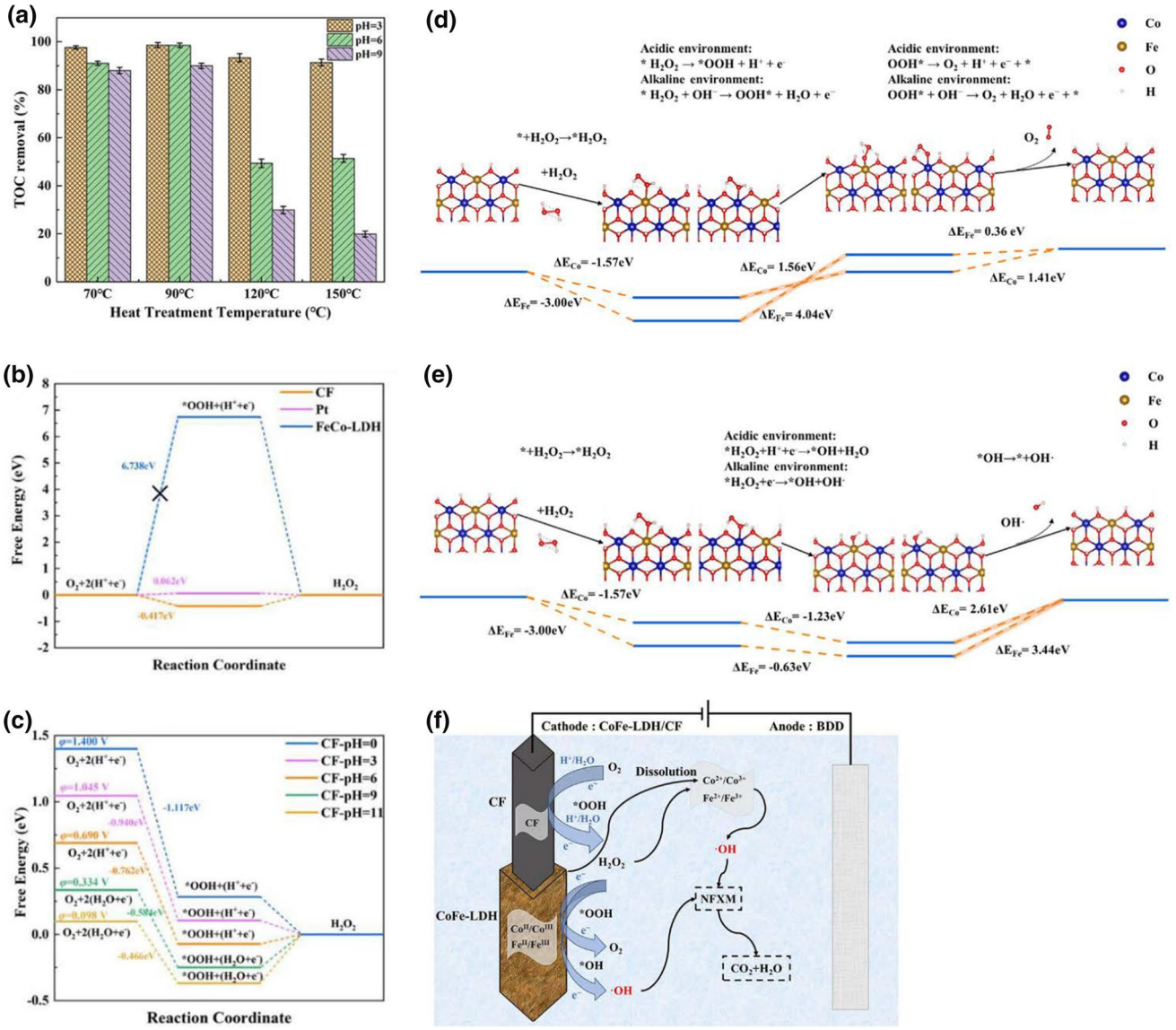

Fig. 4 **a** Comparison of organic compound degradation at different pHs by CoFe-LDH/CF catalysts synthesized at different temperatures, TOC refers to total organic carbon; **b** a free energy diagram of $2e^-$ oxygen reduction reaction on CoFe layered double hydroxides (CoFe-LDH), carbon felt (CF), and Pt (111) at pH = 0; **c** a free energy diagram of $2e^-$ oxygen reduction reaction on carbon felts (CF) at different pHs; **d** geometric structures and potential energies of H_2O_2 activation to ·OH and **e** H_2O_2 decomposition to O_2 on CoFe–LDH; (f) H_2O_2 synthesis, ·OH generation, and a contaminant (NFXM) degradation on CoFe-LDH/CF. Reprinted with permission of (Yu et al. 2021a), Copyright Elsevier

trimetallic carbon composite catalysts may boost catalyst performance in several different ways: (1) in addition to Fe, other metal species can also activate H_2O_2 to generate ·OH; (2) additional metals form redox couples, which facilitate the reduction of Fe(III) to Fe(II), promoting the Fenton reaction; (3) introducing some metals, such as Cu, may create oxygen vacancy, which may reduce adsorbed O_2 to generate $\cdot O_2^-$, and (4) local electronic environment of carbon materials may be tuned by electrons from encapsulated alloy nanoparticles, resulting in the activation of H_2O_2 to ·OH by the 1 e^- pathway.

Transition metal single-atom catalysts

In catalysts containing supported metal nanoparticles, a significant fraction of active sites would be inaccessible to reactants, such as O_2 or H_2O_2 in heterogeneous electro-Fenton processes, limiting their mass-based catalytic activity. Recent studies show that single-atom catalysts with metal nanoparticles downsized to atomically dispersed metal atoms have significantly improved catalytic performance (Zhang et al. 2018; Chen et al. 2019). Several transition metal single-atom catalysts have been applied as bifunctional

catalysts in heterogeneous electro-Fenton processes. For example, Cao et al. (2020b) developed a single-atom catalyst containing Fe anchored on 3D porous carbon using metal–organic framework (Cu/MIL-88B(Fe) as precursors. X-ray absorption spectroscopy and density functional theory calculation results suggested that Fe atoms were more likely captured on defective edges of isolated holes in the porous carbon (Fig. 5a, b). The catalyst demonstrated fast degradation kinetics, 59 times higher than Fe_3O_4 nanoparticles supported on porous carbon. Further, this catalyst selectively absorbed specific organics depending on their charged properties and electron distribution. The authors proposed that the surface-confined ·OH could selectively oxidize absorbed organic compounds. Thus, the catalyst exhibited different degradation selectivity toward various organic compounds, i.e., benzoic acid, phenol, and nitrobenzene (Fig. 5c). Song et al. incorporated Fe atoms into defect-enriched graphene sheets. They found that Fe atoms were anchored on abundant pyridinic-N sites. The synergistic effects of Fe–N and Fe–O sites contributed to the high H_2O_2 synthesis selectivity and efficient organic contaminant (chloramphenicol) removal under extreme pH conditions (pH < 4 or pH > 10) (Song et al. 2021). Zhang et al. (2022a) synthesized a hollow sea-urchin-shaped carbon-anchored Fe single-atom catalyst (SAFe@HSC, see images in Fig. 5d, e) using ZnFe metal–organic framework as precursors. A transmission electron microscopy image shows well-dispersed bright spots (i.e., single Fe atom sites) on the carbon matrix (Fig. 5f). The catalyst containing 1.62 wt.% Fe showed the highest selectivity toward H_2O_2 (Fig. 5g, based on the ring current intensity). When the Fe content increased to 2.04 wt.%, the selectivity toward H_2O_2 decreased due to the formation of Fe nanoparticles. The electron transfer number (n) for oxygen reduction reaction is around 2.8 (Fig. 5h), indicating that besides the dominant $2e^-$ oxygen reduction reaction, $4e^-$ oxygen reduction reaction to H_2O, $3e^-$ to ·OH, and $1e^-$ H_2O_2 to ·OH might also occur. Further, no DMPO (5,5-dimethyl-1-pyrroline N-oxide)-OH electron spin resonance signal was detected on porous carbon without Fe (Fig. 5i). And, the signal decreased a lot when Fe was chelated by 1,10-phenanthroline (Fig. 5j), suggesting that Fe atoms were active sites to activate H_2O_2 to produce ·OH.

Chlorinated organics are difficult to be degraded because their stable C–Cl bond is resistant to reactive oxygen species. Zhao et al. (2021) synthesized a bimetallic single-atom catalyst by anchoring both Fe and Cu on N-doped porous carbon matrix (FeCuSA-NPC). Cu and Fe atoms were atomically coordinated by 4 N atoms in Fe-N_4 and Cu-N_4 sites. Detailed comparisons were carried out among FeCuSA-NPC and single metal element (FeSA-NPC and CuSA-NPC) references and carbon catalyst (NPC) by the degradation of a model contaminant (4-chlorophenol). Figure 5k shows that 95% of 4-chlorophenol was degraded in 60 min on FeCuSA-NPC, 27, 81, 68% on NPC, FeSA-NPC, and CuSA-NPC, respectively. Figure 5l shows that FeSA-NPC had the highest yield of ·OH (116 μmol L^{-1}), higher than that of FeCuSA-NPC (95.9 μmol L^{-1}) and CuSA-NPC (59.6 μmol L^{-1}). These results suggested that the degradation of 4-chlorophenol did not solely depend on ·OH. The degradation of 4-chlorophenol was further compared in Ar-saturated solution, and Fig. 5m shows 100% 4-chlorophenol dechlorination on FeCuSA-NPC, followed by 79.7% on CuSA-NPC, 68.5% on FeSA-NPC, and 50.6% on NPC in 120 min. Density functional theory calculations were used to further compare 4-chlorophenol and O_2 adsorption on Fe-N_4 and Cu-N_4 sites. O_2 preferred to be adsorbed on Fe-N_4, while the 4-chlorophenol adsorption on Cu-N_4 was favorable. Thus, the authors proposed that atomic Fe improved the $2e^-$ oxygen reduction reaction on N-doped carbon and facilitated the activation of H_2O_2 to ·OH, whereas atomic Cu not only promoted H_2O_2 generation but also accelerated the dichlorination of 4-chlorophenol (Fig. 5n).

Metal composite catalysts without carbon

Other than relying on carbon materials to catalyze the synthesis of H_2O_2, some studies have demonstrated that metal composite catalysts without carbon materials can achieve the same. The synthesis and activation of H_2O_2 may occur on the same or different metal active sites in metal composite catalysts. Tuning the ratio among metal species can affect their catalytic performance. For example, Ross et al. (2021) reported compositionally tuned trimetallic thiosphinels ($CuCo_{2-x}Ni_xS_4$, $0 \le x \le 1.2$) as a bifunctional catalyst. Transition metal sulfides, such as $CuCo_2S_4$, have shown activity for $2e^-$ oxygen reduction reaction (Zhao et al. 2016b). Ni was used to substitute some Co in $CuCo_2S_4$ to enhance its oxygen reduction reaction activity. Notably, the authors found that an acid treatment step in 0.05 M H_2SO_4 solution was critical for ·OH generation. The leached soluble Cu^+ reacted with H_2O_2 to produce ·OH. In another study, Zhang et al. (2022b) reported a core–shell Fe@Fe_2O_3-CeO_2 composite catalyst. However, it should be noted that an activated carbon filter was used in the cathode; thus, carbon materials might still contribute to H_2O_2 synthesis via $2e^-$ oxygen reduction reaction. A previous study has proposed that H_2O_2 synthesis can also be directly catalyzed by Fe^0 (Eq. 26) (Shi et al. 2014). Thus, the authors proposed that Fe^0 in this catalyst promoted H_2O_2 generation, and additional Fe^{2+} further acted as the Fenton reagents for ·OH production. Additionally, the synergistic effects between Fe(II)/Fe(III) and Ce(III)/Ce(IV) accelerated the generation of ·OH from H_2O_2, similar to bimetallic catalysts discussed earlier.

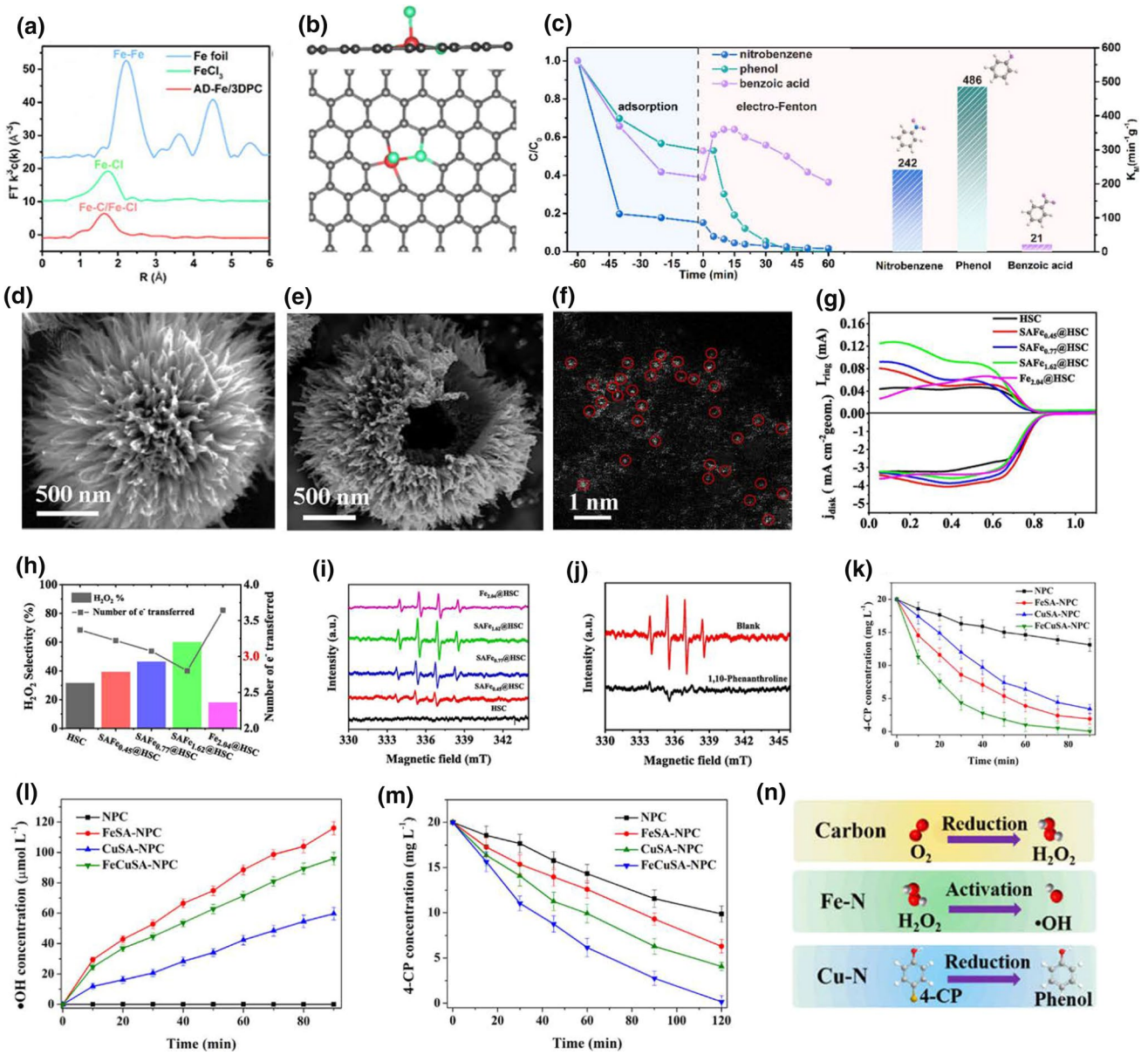

Fig. 5 **a** Fourier-transformed X-ray absorption spectra in *R* space at Fe K-edge for the single-atom Fe catalyst (AD-Fe/3DPC), Fe foil, and $FeCl_3$; **b** a density functional theory optimized atomic model of the C_3-Fe sited with an adsorbed Cl_2 (the red, light green and gray atoms represent Fe, Cl, and C atoms, respectively); and **c** the adsorption and degradation of different organic contaminants from an initial concentration of 0.12 mM and the corresponding reaction constant K_M on the right. Reprinted with permission of (Cao et al. 2020b), *Copyright ACS*. **d**–**e** Scanning electron microscope images and **f** a transmission electron microscope image of a hollow sea-urchin-shaped carbon-anchored single-atom Fe catalyst; **g** Polarization curves and ring electron current density (for H_2O_2 detection) at 1600 rpm for Fe single-atom catalysts anchored in hollow sea-urchin-shaped carbon ($SAFe_{0.45}$@HSC, $SAFe_{0.77}$@HSC, $SAFe_{1.62}$@HSC), hollow sea-urchin-shaped carbon (HSC) and Fe nanoparticles supported on hollow sea-urchin-shaped carbon ($Fe_{2.04}$@HSC); **h** electron transfer electron number (*n*) of oxygen reduction reaction and H_2O_2 selectivity; **i** DMPO (5,5-dimethyl-1-pyrroline N-oxide) spin-trapping electron spin resonance spectra (oxygen reduction reaction for 20 min), **j** DMPO spin-trapping electron spin resonance spectra in 5 mM 1,10-phenanthroline or blank. Reprinted with permission of (Zhang et al. 2022a), *Copyright Elsevier*. **k** 4-chlorophenol degradation on single-atom Fe and Cu anchored on N-doped porous carbon matrix (FeCuSA-NPC) and reference catalysts; **l** ·OH concentration as a function of reaction time; **m** 4-chlorophenol degradation by electrochemical reduction on different catalysts; **n** proposed reaction mechanism of 4-chlorophenol degradation on FeCuSA-NPC, carbon for H_2O_2 generation, Fe–N for H_2O_2 activation, and Cu–N for dichlorination. Reprinted with permission of (Zhao et al. 2021), *Copyright ACS*

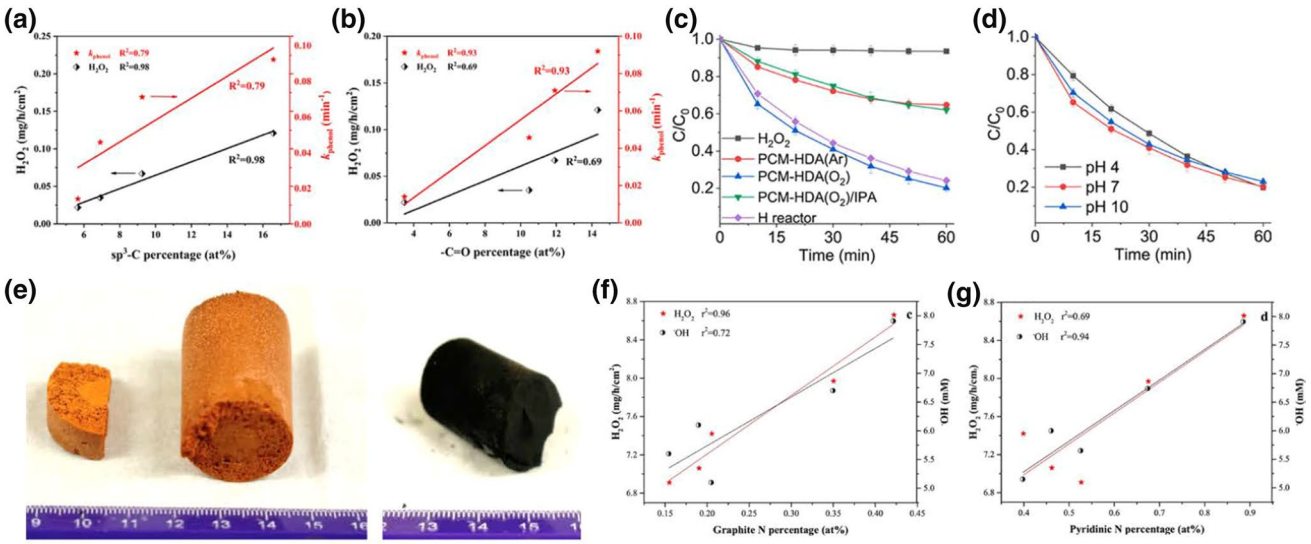

Fig. 6 **a**, **b** Dependences of H_2O_2 yield and k_{phenol} and on the percentage of sp^3-C and –C=O on oxidized carbon nanotubes. Reprinted with permission of (Qin et al. 2021), *Copyright Elsevier*. **c** Degradation of napropamide by porous carbon monoliths under different reaction conditions; **d** at different pHs; **e** Photographs of porous carbon monoliths before and after carbonization. Reprinted with permission of (Yu et al. 2021b), *Copyright Elsevier*. **f** Correlations between the yield of H_2O_2 and concentration of ·OH with the percentage of graphite N, and **g** the percentage of pyridinic N. Reprinted with permission of (Su et al. 2019), *Copyright Elsevier*

$$Fe^0 + O_2 + 2H^+ \rightarrow Fe^{2+} + H_2O_2 \quad (26)$$

Metal-free carbonaceous catalysts

The concentration of Fe^{2+} in homogenous Fenton processes is at its maximum at pH 2.8 (Brillas et al. 2009). Adjusting solution pH and treating Fe sludge would dramatically increase the operating costs of Fenton processes. Although heterogeneous catalysts containing trapped or bonded metal species significantly limit the loss of metal ions and improve catalyst stability, leaching metal ions from metal-containing catalysts in acidic conditions cannot be avoided entirely. Thus, there is a vital interest in developing metal-free carbonaceous catalysts for heterogeneous electro-Fenton processes. Early studies have already found that carbon materials, such as graphite, activated carbon, and carbon black, are capable of catalyzing H_2O_2 synthesis and activating H_2O_2 to generate ·OH (Georgi and Kopinke 2005). However, their activity is often much lower than metal-based catalysts. Extensive efforts have been devoted to understanding the reaction mechanisms of carbon catalysts so their activity can be improved (Liu et al. 2015b; Iglesias et al. 2018; Kim et al. 2018; Lu et al. 2018; Hu et al. 2021a, 2021b). In general, several parameters have been found to influence their activity strongly. (1) High electrical conductivity is essential to facilitate electron transfer. (2) A high surface area is beneficial to host more catalytic active activity sites. (3) Suitable porosity can influence mass transfer and selectivity. For example, Iglesias et al. showed that micropores decreased the residence time of H_2O_2 in catalysts, which prevented its further reduction to water and improved the selectivity toward H_2O_2. (4) Heteroatom dopings such as O, N, B, and defects in carbon materials strongly affect catalytic activity. However, it is still under debates the exact role of different doping or defect configurations. We introduce several recent studies on heteroatom-doped carbon materials as bifunctional catalysts below.

Qin et al. (2021) used oxidized carbon nanotubes as a bifunctional catalyst for phenol degradation under neutral conditions. The O doping was introduced by acid (HNO_3 and H_2SO_4) treatment at 40 to 100 °C for 1 h. The H_2O_2 yield displayed a linear relationship with the percentage of sp^3-C bond on carbon nanotubes (Fig. 6a). Similarly, the degradation rate constants of phenol (k_{phenol}) showed a positive linear relationship with the percentage of –C=O group on carbon nanotube surfaces (Fig. 6b). Yu et al. (2021b) used 1,6-hexamethylene diamine as a precursor to synthesize porous carbon monoliths, demonstrating an H_2O_2 yield 374% higher than carbon black. The catalytic activity was attributed to O functional groups and sp^3 structural defects. Figure 6c shows that porous carbon monoliths could not cleave H_2O_2 without applied potentials, and it activated H_2O_2 via the 1 e^- pathway (Eqs. 15–16). Adding isopropanol would quickly quench ·OH generated. Porous carbon monoliths worked efficiently over a wide pH range (4–10) (Fig. 6d). Porous carbon monoliths also demonstrated excellent mechanical strength, serving as free-standing electrodes without adding non-conductive binders in electrode fabrication (Fig. 6e).

Besides O doping, N has a similar atomic size to C with 5 valence electrons, easily forming covalent bonds within the carbon matrix and inducing positive charges on adjacent carbon atoms. N doping carbon materials have shown catalytic activities for H_2O_2 generation and activation. Various N-containing molecules (i.e., ammonium nitrate and melamine) and polymers (i.e., polyaniline and polydopamine (PDA) have been used as N precursors to synthesize N-doped carbon catalysts (Iglesias et al. 2018; Yang et al. 2018b, 2019; Haider et al. 2019; Su et al. 2019, 2020). N atoms in the carbon matrix can form different N species, such as pyridinic N, pyrrolic N, graphitic N, and pyridinic N-oxide. The abundance of these N species has been tailored by N and C precursors, pyrolysis temperature, and pore formation agents (i.e., KOH). It is still controversial on their catalytic roles. Some studies showed correlations between graphitic N and H_2O_2 concentration (Fig. 6f) or between pyridinic N and $^{\cdot}OH$ concentration (Fig. 6g), suggesting that graphitic N could be active for H_2O_2 synthesis and pyridinic N could activate H_2O_2 to generate $^{\cdot}OH$ (Su et al. 2019). Further, boron (B)-doped graphene was also used as a bifunctional catalyst (Wu et al. 2019; Chen et al. 2021). B atoms with positive charges ($–BC_3$) could serve as active sites to cleave the O–O bond in H_2O_2, while electrophilic B sites (e.g., $–BC_2O$, $–BCO_2$), mainly located at the edge and defect sites, could act as active sites for O_2 absorption and H_2O_2 generation.

Other approaches to improve performance

Beyond the design of electrocatalysts themselves, recent studies also demonstrated several other approaches to improve the performance of heterogeneous electro-Fenton processes. They usually improve the mass transfer of reactants or combine catalytic reactions with other processes. In this session, we briefly describe these approaches.

First, materials with large specific surfaces, such as activated carbon, have been widely used as adsorbents to absorb various contaminates. The lifetime (~ 20 ns) and diffusion length (~ 6 nm) of $^{\cdot}OH$ are usually very short (Georgi and Kopinke 2005). Thus, the efficiency of $^{\cdot}OH$ in heterogeneous electro-Fenton processes could be improved if contaminant molecules have been adsorbed on the surface of catalysts close to where $^{\cdot}OH$ is generated. Bifunctional catalysts with large specific surfaces have been used to combine their catalyst and adsorbent roles. Figure 7a illustrates the degradation of Reactive Blue 19 on an activated carbon-based bifunctional catalyst (Zhou et al. 2019). Reactive Blue 19 was adsorbed on the surface and inside pores of activated carbon. H_2O_2 was generated on active sites within the pores of activated carbon, including the micro-, meso-, and macropores, by the 2 e^- oxygen reduction reaction. H_2O_2 was partially released into the bulk of the solution and was activated on the carbon surface to generate $^{\cdot}OH$. Some H_2O_2 was activated to $^{\cdot}OH$ inside the pores, which attacked Reactive Blue 19 adsorbed inside the pores.

Second, O_2 has low water solubility, limiting the 2 e^- oxygen reduction reaction. Rather than bubbling O_2 into aqueous solutions in common studies, Yu et al. (2014) proposed a rotating disk reactor with two rotating graphite felt cathodes (Fig. 7b). At the low rotation speed of 10 rpm, the total organic carbon removal efficiency was threefold higher than the condition without rotation.

Third, the conversion from O_2 to reactive oxygen species occurs at triple-phase interfaces. O_2 is usually supplied from the gas phase; the reactions take place on the surface of solid catalysts, while the resulting reactive oxygen species are released into the liquid phase. Thus, interface properties are expected to strongly influence reaction kinetics and the mass transfer of reactants and reaction products (Tang et al. 2018; Wang et al. 2019). Gas diffusion electrodes have a porous, hydrophobic, and hydrophilic structure, which allow sufficient O_2 delivered to solid–liquid–gas interfaces (Reis et al. 2012; Luo et al. 2015; Lu et al. 2021; Xu et al. 2021). As illustrated in Fig. 7c, carbon felts modified by polytetrafluoroethylene served as the hydrophobic gas diffusion layer and the current collector, while catalysts were loaded on the other side of the carbon felts exposed to water (Zhang et al. 2020). Gas diffusion electrodes often brought significant performance enhancement because they enabled much higher O_2 concentration and faster mass transfer of O_2 molecules at reaction interfaces (Reis et al. 2012; Luo et al. 2015; Lu et al. 2021; Xu et al. 2021).

Fourth, in some electro-Fenton processes, H_2O_2 was activated by Fe^{2+} (Eq. 12), which requires the regeneration of Fe^{2+} from Fe^{3+} on cathodes (Eq. 13). The optimal potential required for H_2O_2 synthesis (e.g., − 0.5 V) may not be the same for Fe^{2+} reduction. The high potential for the 2e^- oxygen reduction reaction might lead to Fe film formation on cathodes. Liang et al. (2021) proposed to adjust the potential applied on cathodes to balance the efficiency of the 2e^- oxygen reduction reaction and Fe^{2+} reduction. Under the optimum potential of − 0.1 V applied on the gas diffusion electrode, high H_2O_2 production and slow Fe^{2+} consumption rates were achieved (Fig. 7d).

Fifth, to avoid using bifunctional catalysts, Wang et al. (2021a) proposed a dual-cathode reactor to separate H_2O_2 synthesis and activation (Fig. 7e). Poly(3,4-ethylenedioxythiophene) modified carbon cloth (PEDOT/CC) was applied as the catalyst for H_2O_2 synthesis, and a stainless steel mesh was applied to activate H_2O_2 to $^{\cdot}OH$. The PEDOT/CC cathode yielded the highest H_2O_2 concentration (243.1 mg L^{-1}) at − 0.9 V, while the stainless-steel-mesh cathode can convert the in situ generated H_2O_2 to $^{\cdot}OH$ at the highest rate at − 0.8 V. The dual cathode reactor showed a higher removal efficiency of RhB under these two different potentials,

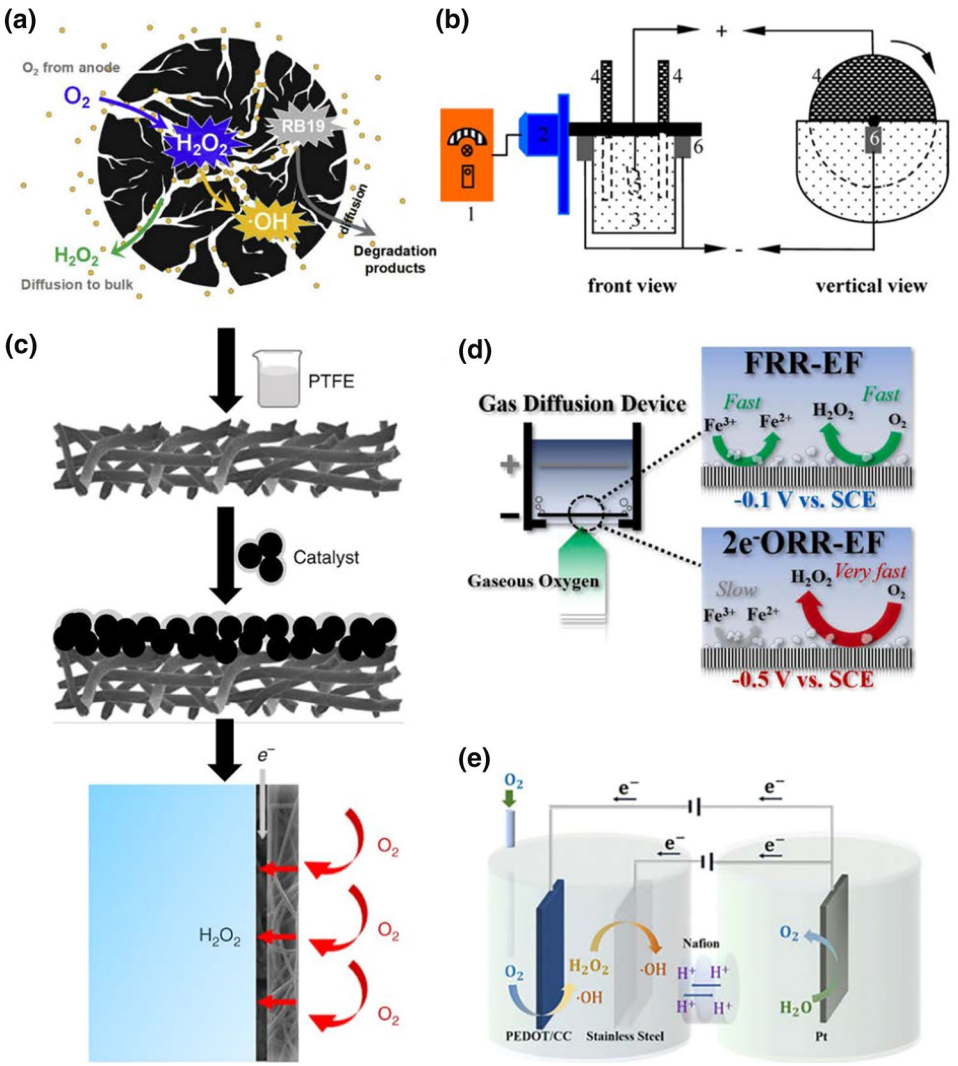

Fig. 7 **a** Mechanism of an activated carbon-based bifunctional catalyst for simultaneous Reactive Blue 19 (RB19) adsorption and degradation. Reprinted with permission of (Zhou et al. 2019), *Copyright Elsevier*. **b** A rotating disk reactor with two rotating graphite felt cathodes. Reprinted with permission of (Yu et al. 2014), *Copyright ACS*. **c** Carbon felts modified by polytetrafluoroethylene (PTFE) served as the hydrophobic gas diffusion layer and the current collector, while catalysts loaded on the other side of the carbon felts exposed to water. Reprinted with permission of (Zhang et al. 2020), *Copyright Springer Nature*. **d** Adjusting the potential applied on cathodes to balance $2e^-$ oxygen reduction reaction (ORR) and Fe^{2+} reduction reaction (FRR) in electro-Fenton (EF) process. Reprinted with permission of (Liang et al. 2021), *Copyright Elsevier*. **e** A dual-cathode reactor to separate H_2O_2 synthesis and activation on two cathodes. PEDOT/CC refers to Poly(3,4-ethylenedioxythiophene) modified carbon cloth. Reprinted with permission of (Wang et al. 2021a), *Copyright National Academy of Sciences*

compared to PEDOT/CC cathode alone or stainless-steel-mesh cathode alone, respectively.

Conclusion

Bifunctional catalysts in heterogeneous electro-Fenton processes can synthesize and activate H_2O_2 simultaneously, which has the potential to overcome the shortcomings of conventional Fenton processes used in water and wastewater treatment. Rationally designed bifunctional catalysts are expected to provide high activity and selectivity, work in a wide pH range, and have excellent stability for reuses in multiple reaction cycles. This review has summarized recent progress in developing various bifunctional catalysts to achieve this goal. Although remarkable progress has been achieved, there are still significant gaps for practical applications. We propose the following areas to be priorities in upcoming research studies:

1. There is still no consensus on the reaction mechanisms of converting O_2 to reactive oxygen species. It is widely recognized that different catalytic active sites might be required for H_2O_2 synthesis via the 2 e^- oxygen reduction reaction and H_2O_2 activation toward $^{\cdot}OH$. However, it is unclear what specific active sites could achieve a high selectivity of the 2 e^- oxygen reduction reaction over the 4 e^- oxygen reduction reaction or catalyze the formation of $^{\cdot}OH$ from H_2O_2 rather than producing H_2O or O_2. Breaking linear scaling relationships among the adsorption energy of different O intermediates on catalyst surfaces may be the key to achieving high selectivity toward a specific reaction pathway. It is also unclear what the consequence is if such selective catalytic sites are put close together on a bifunctional catalyst. In situ spectroscopic studies of model catalysts with well-

defined catalytic sites in combination with theoretical calculations should be used to resolve these puzzles. The improved understanding can guide the design of new catalysts.

2. In electro-Fenton processes, the generation of ·OH on bifunctional catalysts often involves two steps. First, H_2O_2 is synthesized on active site 1 and then desorb from the active site ($O_2 \rightarrow *O_2 \rightarrow *H_2O_2 \rightarrow H_2O_2$). Next, H_2O_2 is adsorbed on active site 2 to be activated in situ to generate ·OH ($H_2O_2 \rightarrow *H_2O_2 \rightarrow *OH \rightarrow \cdot OH$). The mass transfer is usually the rate limit step in the whole process. It could be more efficient to design a bifunctional catalyst with active sites that can catalyze the generation of ·OH from O_2 directly via the 3 e^- oxygen reduction reaction: $O_2 \rightarrow *O2 \rightarrow *H_2O_2 \rightarrow *OH \rightarrow \cdot OH$. Both theoretical and experimental studies will be needed to verify whether such a process would be feasible on a suitable catalyst.
3. The desorption of generated surface-bond ·OH has a high energy barrier, while its lifetime is short (~ 20 ns). Further, its diffusion length is also short (~ 6 nm). The desorption of ·OH is a rate-limiting step in the electro-Fenton process. It may be helpful to develop tri-functional catalysts which enable strong bondings between organic molecules and surface-bonded ·OH, eliminating the ·OH desorption step. Innovative catalyst designs will be needed to realize such a catalyst.
4. Heterogeneous electro-Fenton processes used for water treatment likely require many bifunctional catalysts. Although catalysts with complex nanoscale structures have demonstrated superior performance in research labs, their complex synthesis methods and high cost might prohibit their adoption in practical applications. It is essential to carry out comprehensive evaluations of new catalysts to narrow the gap between fundamental catalyst research and practical applications. Thus, an important task should be balancing catalyst performance and costs.
5. Since heterogeneous electro-Fenton processes occur at triple-phase interfaces, catalyst interface designs and reactor designs are expected to play critical roles to enable the efficient mass transfer of reactants and reaction products, similar to what we have reviewed earlier. More research from fundamental understanding, electrode material design, and process simulation would be required to deliver the desired superior performances.
6. Fast catalyst performance degradation is a critical challenge for many catalysts in heterogeneous electro-Fenton processes. Metal leaching, surface fouling, chemical property changes, and structural destruction can significantly shorten catalyst service life. More efforts are required to understand the degradation mechanism of bifunctional catalysts and eventually design more stable catalysts with long service life.

Although there are still many challenges ahead, we believe that more bifunctional catalysts will be applied in heterogeneous electro-Fenton processes with improved fundamental understandings and innovative engineering designs. They will sustainably produce H_2O_2 and ·OH with only O_2 and electricity consumed. They can play a critical role in addressing environmental challenges globally. This exciting area calls for more research to resolve current challenges.

Acknowledgements This work was funded by the Australian Government Department of Industry, Science, Energy and Resource (Innovative Manufacturing Cooperative Research Centre).

Funding Open Access funding enabled and organized by CAUL and its Member Institutions. The authors have not disclosed any funding.

Declarations

Conflict of interest The authors declare that they have no known competing financial interests or personal relationships that could have appeared to influence the work reported in this paper.

References

Brillas E, Sirés I, Oturan MA (2009) Electro-Fenton process and related electrochemical technologies based on Fenton's reaction chemistry. Chem Rev 109(12):6570–6631. https://doi.org/10.1021/cr900136g

Caban M, Stepnowski P (2021) How to decrease pharmaceuticals in the environment? A review. Environ Chem Lett 19(4):3115–3138. https://doi.org/10.1007/s10311-021-01194-y

Cao P, Quan X, Zhao K, Chen S, Yu H, Niu J (2020a) Selective electrochemical H_2O_2 generation and activation on a bifunctional catalyst for heterogeneous electro-Fenton catalysis. J Hazard Mater 382:121102. https://doi.org/10.1016/j.jhazmat.2019.121102

Cao P, Quan X, Zhao K, Chen S, Yu H, Su Y (2020b) High-efficiency electrocatalysis of molecular oxygen toward hydroxyl radicals enabled by an atomically dispersed iron catalyst. Environ Sci Technol 54(19):12662–12672. https://doi.org/10.1021/acs.est.0c03614

Chen ZW, Chen LX, Yang CC, Jiang Q (2019) Atomic (single, double, and triple atoms) catalysis: frontiers, opportunities, and challenges. J Mater Chem A 7(8):3492–3515. https://doi.org/10.1039/C8TA11416A

Chen X, Wang L, Sun W, Yang Z, Jin J, You D, Liu G (2021) Enhanced electrochemical advanced oxidation on boride activated carbon: the influences of boron groups. Electrochim Acta 400:139462. https://doi.org/10.1016/j.electacta.2021.139462

Chen X, Teng W, Fan J, Chen Y, Ma Q, Xue Y, Zhang C, Zhang W-x (2022) Enhanced degradation of micropollutants over iron-based electro-Fenton catalyst: cobalt as an electron modulator in mesochannels and mechanism insight. J Hazard Mater 427:127896. https://doi.org/10.1016/j.jhazmat.2021.127896

Cheng M, Lai C, Liu Y, Zeng G, Huang D, Zhang C, Qin L, Hu L, Zhou C, Xiong W (2018) Metal-organic frameworks for highly efficient heterogeneous Fenton-like catalysis. Coord Chem Rev 368:80–92. https://doi.org/10.1016/j.ccr.2018.04.012

Cheng S, Zheng H, Shen C, Jiang B, Liu F, Li A (2021) Hierarchical iron phosphides composite confined in ultrathin carbon layer as effective heterogeneous electro-Fenton catalyst with prominent stability and catalytic activity. Adv Func Mater 31(48):2106311. https://doi.org/10.1002/adfm.202106311

Chong MN, Jin B, Chow CWK, Saint C (2010) Recent developments in photocatalytic water treatment technology: a review. Water Res 44(10):2997–3027. https://doi.org/10.1016/j.watres.2010.02.039

Dai Y, Yao Y, Li M, Fang X, Shen C, Li F, Liu Y (2022) Carbon nanotube filter functionalized with MIL-101(Fe) for enhanced flow-through electro-Fenton. Environ Res 204:112117. https://doi.org/10.1016/j.envres.2021.112117

Divyapriya G, Nidheesh PV (2020) Importance of Graphene in the Electro-Fenton Process. ACS Omega 5(10):4725–4732. https://doi.org/10.1021/acsomega.9b04201

Dong P, Wang H, Liu W, Wang S, Wang Y, Zhang J, Lin F, Wang Y, Zhao C, Duan X, Wang S, Sun H (2021) Quasi-MOF derivative-based electrode for efficient electro-Fenton oxidation. J Hazard Mater 401:123423. https://doi.org/10.1016/j.jhazmat.2020.123423

Dsikowitzky L, Schwarzbauer J (2014) Industrial organic contaminants: identification, toxicity and fate in the environment. Environ Chem Lett 12(3):371–386. https://doi.org/10.1007/s10311-014-0467-1

Dung NT, Duong LT, Hoa NT, Thao VD, Ngan LV, Huy NN (2022) A comprehensive study on the heterogeneous electro-Fenton degradation of tartrazine in water using CoFe2O4/carbon felt cathode. Chemosphere 287:132141. https://doi.org/10.1016/j.chemosphere.2021.132141

Ganiyu SO, Le Huong TX, Bechelany M, Esposito G, van Hullebusch ED, Oturan MA, Cretin M (2017) A hierarchical CoFe-layered double hydroxide modified carbon-felt cathode for heterogeneous electro-Fenton process. J Mater Chem A 5(7):3655–3666. https://doi.org/10.1039/C6TA09100H

Gao G, Zhang Q, Hao Z, Vecitis CD (2015) Carbon nanotube membrane stack for flow-through sequential regenerative electro-Fenton. Environ Sci Technol 49(4):2375–2383. https://doi.org/10.1021/es505679e

Garcia-Segura S, Brillas E (2011) Mineralization of the recalcitrant oxalic and oxamic acids by electrochemical advanced oxidation processes using a boron-doped diamond anode. Water Res 45(9):2975–2984. https://doi.org/10.1016/j.watres.2011.03.017

Georgi A, Kopinke F-D (2005) Interaction of adsorption and catalytic reactions in water decontamination processes: Part I. Oxidation of organic contaminants with hydrogen peroxide catalyzed by activated carbon. Appl Catal B Environ 58(1):9–18. https://doi.org/10.1016/j.apcatb.2004.11.014

Guo X, Lin S, Gu J, Zhang S, Chen Z, Huang S (2019) Simultaneously achieving high activity and selectivity toward two-electron O_2 electroreduction: the power of single-atom catalysts. ACS Catal 9(12):11042–11054. https://doi.org/10.1021/acscatal.9b02778

Haider MR, Jiang W-L, Han J-L, Sharif HMA, Ding Y-C, Cheng H-Y, Wang A-J (2019) In-situ electrode fabrication from polyaniline derived N-doped carbon nanofibers for metal-free electro-Fenton degradation of organic contaminants. Appl Catal B 256:117774. https://doi.org/10.1016/j.apcatb.2019.117774

He H, Zhou Z (2017) Electro-Fenton process for water and wastewater treatment. Crit Rev Environ Sci Technol 47(21):2100–2131. https://doi.org/10.1080/10643389.2017.1405673

Hou X, Huang X, Jia F, Ai Z, Zhao J, Zhang L (2017) Hydroxylamine promoted goethite surface fenton degradation of organic pollutants. Environ Sci Technol 51(9):5118–5126. https://doi.org/10.1021/acs.est.6b05906

Hu C, Paul R, Dai Q, Dai L (2021a) Carbon-based metal-free electrocatalysts: from oxygen reduction to multifunctional electrocatalysis. Chem Soc Rev 50(21):11785–11843. https://doi.org/10.1039/D1CS00219H

Hu CG, Dai QB, Dai LM (2021b) Multifunctional carbon-based metal-free catalysts for advanced energy conversion and storage. Cell Rep Phys Sci. https://doi.org/10.1016/j.xcrp.2021b.100328

Hu J, Wang S, Yu J, Nie W, Sun J, Wang S (2021c) Duet Fe_3C and FeN_x sites for H_2O_2 generation and activation toward enhanced electro-fenton performance in wastewater treatment. Environ Sci Technol 55(2):1260–1269. https://doi.org/10.1021/acs.est.0c06825

Hu T, Deng F, Feng H, Zhang J, Shao B, Feng C, Tang W, Tang L (2021d) Fe/Co bimetallic nanoparticles embedded in MOF-derived nitrogen-doped porous carbon rods as efficient heterogeneous electro-Fenton catalysts for degradation of organic pollutants. Appl Mater Today 24:101161. https://doi.org/10.1016/j.apmt.2021.101161

Huang Z-H, Liu J-M, Ji Z-Y, Yuan P, Guo X-F, Li S-M, Li H, Yuan J-S (2022) Effective and continuous degradation of levofloxacin via the graphite felt electrode loaded with Fe3O4. Sep Purif Technol 281:119902. https://doi.org/10.1016/j.seppur.2021.119902

Hussain S, Aneggi E, Goi D (2021) Catalytic activity of metals in heterogeneous Fenton-like oxidation of wastewater contaminants: a review. Environ Chem Lett 19(3):2405–2424. https://doi.org/10.1007/s10311-021-01185-z

Iglesias D, Giuliani A, Melchionna M, Marchesan S, Criado A, Nasi L, Bevilacqua M, Tavagnacco C, Vizza F, Prato M, Fornasiero P (2018) N-Doped graphitized carbon nanohorns as a forefront electrocatalyst in highly selective O2 reduction to H2O2. Chem 4(1):106–123. https://doi.org/10.1016/j.chempr.2017.10.013

Kim HW, Ross MB, Kornienko N, Zhang L, Guo J, Yang P, McCloskey BD (2018) Efficient hydrogen peroxide generation using reduced graphene oxide-based oxygen reduction electrocatalysts. Nat Catal. https://doi.org/10.1038/s41929-018-0044-2

Kulkarni A, Siahrostami S, Patel A, Nørskov JK (2018) Understanding catalytic activity trends in the oxygen reduction reaction. Chem Rev 118(5):2302–2312. https://doi.org/10.1021/acs.chemrev.7b00488

Liang J, Xiang Q, Lei W, Zhang Y, Sun J, Zhu H, Wang S (2021) Ferric iron reduction reaction electro-Fenton with gas diffusion device: a novel strategy for improvement of comprehensive efficiency in electro-Fenton. J Hazard Mater 412:125195. https://doi.org/10.1016/j.jhazmat.2021.125195

Lin L, Miao N, Wallace GG, Chen J, Allwood DA (2021) Engineering carbon materials for electrochemical oxygen reduction reactions. Adv Energy Mater 11(32):2100695. https://doi.org/10.1002/aenm.202100695

Liu Y, Chen S, Quan X, Yu H, Zhao H, Zhang Y (2015a) Efficient mineralization of perfluorooctanoate by electro-Fenton with H_2O_2

electro-generated on hierarchically porous carbon. Environ Sci Technol 49(22):13528–13533. https://doi.org/10.1021/acs.est.5b03147

Liu Y, Quan X, Fan X, Wang H, Chen S (2015b) High-yield electrosynthesis of hydrogen peroxide from oxygen reduction by hierarchically porous carbon. Angew Chem Int Ed 54(23):6837–6841. https://doi.org/10.1002/anie.201502396

Liu K, Yu JC-C, Dong H, Wu JCS, Hoffmann MR (2018) Degradation and mineralization of carbamazepine using an electro-Fenton reaction catalyzed by magnetite nanoparticles fixed on an electrocatalytic carbon fiber textile cathode. Environ Sci Technol 52(21):12667–12674. https://doi.org/10.1021/acs.est.8b03916

Liu K, Yu M, Wang H, Wang J, Liu W, Hoffmann MR (2019) Multiphase porous electrochemical catalysts derived from iron-based metal-organic framework compounds. Environ Sci Technol 53(11):6474–6482. https://doi.org/10.1021/acs.est.9b01143

Liu X, Yu H, Ji J, Chen Z, Ran M, Zhang J, Xing M (2021a) Graphene oxide-supported three-dimensional cobalt-nickel bimetallic sponge-mediated peroxymonosulfate activation for phenol degradation. ACS ES&T Engineering 1(12):1705–1714. https://doi.org/10.1021/acsestengg.1c00307

Liu Y, Yang Y, Miao W, Du N, Wang D, Qin H, Mao S, Ostrikov KK (2021b) Bifunctional catalytic cooperativity on nanoedge: oriented Ce–Fe bimetallic fenton electrocatalysts for organic pollutant control. ACS ES&T Engineering 1(12):1618–1632. https://doi.org/10.1021/acsestengg.1c00149

Liu Y, Zhao Y, Wang J (2021c) Fenton/Fenton-like processes with *in-situ* production of hydrogen peroxide/hydroxyl radical for degradation of emerging contaminants: advances and prospects. J Hazard Mater 404:124191. https://doi.org/10.1016/j.jhazmat.2020.124191

Liu Z, Wan J, Ma Y, Wang Y (2021d) In situ synthesis of FeOCl@MoS_2 on graphite felt as novel electro-Fenton cathode for efficient degradation of antibiotic ciprofloxacin at mild pH. Chemosphere 273:129747. https://doi.org/10.1016/j.chemosphere.2021.129747

Lu J, Liu X, Chen Q, Zhou J (2021) Coupling effect of nitrogen-doped carbon black and carbon nanotube in assembly gas diffusion electrode for H_2O_2 electro-generation and recalcitrant pollutant degradation. Sep Purif Technol 265:118493. https://doi.org/10.1016/j.seppur.2021.118493

Lu Z, Chen G, Siahrostami S, Chen Z, Liu K, Xie J, Liao L, Wu T, Lin D, Liu Y, Jaramillo TF, Nørskov JK, Cui Y (2018) High-efficiency oxygen reduction to hydrogen peroxide catalysed by oxidized carbon materials. Nat Catal 1(2):156–162. https://doi.org/10.1038/s41929-017-0017-x

Luo H, Li C, Wu C, Zheng W, Dong X (2015) Electrochemical degradation of phenol by in situ electro-generated and electro-activated hydrogen peroxide using an improved gas diffusion cathode. Electrochim Acta 186:486–493. https://doi.org/10.1016/j.electacta.2015.10.194

Mohammad AW, Teow YH, Ang WL, Chung YT, Oatley-Radcliffe DL, Hilal N (2015) Nanofiltration membranes review: Recent advances and future prospects. Desalination 356:226–254. https://doi.org/10.1016/j.desal.2014.10.043

Montoya-Rodríguez DM, Serna-Galvis EA, Ferraro F, Torres-Palma RA (2020) Degradation of the emerging concern pollutant ampicillin in aqueous media by sonochemical advanced oxidation processes - Parameters effect, removal of antimicrobial activity and pollutant treatment in hydrolyzed urine. J Environ Manag 261:110224. https://doi.org/10.1016/j.jenvman.2020.110224

Munoz M, de Pedro ZM, Casas JA, Rodriguez JJ (2015) Preparation of magnetite-based catalysts and their application in heterogeneous Fenton oxidation—a review. Appl Catal B 176–177:249–265. https://doi.org/10.1016/j.apcatb.2015.04.003

Oturan MA, Peiroten J, Chartrin P, Acher AJ (2000) Complete destruction of p-nitrophenol in aqueous medium by electro-Fenton method. Environ Sci Technol 34(16):3474–3479. https://doi.org/10.1021/es990901b

Oturan N, Panizza M, Oturan MA (2009) Cold incineration of chlorophenols in aqueous solution by advanced electrochemical process electro-Fenton. Effect of number and position of chlorine atoms on the degradation kinetics. J Phys Chem A 113(41):10988–10993. https://doi.org/10.1021/jp9069674

Pi L, Cai J, Xiong L, Cui J, Hua H, Tang D, Mao X (2020) Generation of H_2O_2 by on-site activation of molecular dioxygen for environmental remediation applications: A review. Chem Eng J 389:123420. https://doi.org/10.1016/j.cej.2019.123420

Pignatello JJ, Oliveros E, MacKay A (2006) Advanced oxidation processes for organic contaminant destruction based on the Fenton reaction and related chemistry. Crit Rev Environ Sci Technol 36(1):1–84. https://doi.org/10.1080/10643380500326564

Qin X, Zhao K, Quan X, Cao P, Chen S, Yu H (2021) Highly efficient metal-free electro-Fenton degradation of organic contaminants on a bifunctional catalyst. J Hazard Mater 416:125859. https://doi.org/10.1016/j.jhazmat.2021.125859

Qiu S, Wang Y, Wan J, Ma Y, Yan Z, Yang S (2021) Enhanced electro-Fenton catalytic performance with in-situ grown Ce/Fe@NPC-GF as self-standing cathode: Fabrication, influence factors and mechanism. Chemosphere 273:130269. https://doi.org/10.1016/j.chemosphere.2021.130269

Reis RM, Beati AAGF, Rocha RS, Assumpção MHMT, Santos MC, Bertazzoli R, Lanza MRV (2012) Use of gas diffusion electrode for the in situ generation of hydrogen peroxide in an electrochemical flow-by reactor. Ind Eng Chem Res 51(2):649–654. https://doi.org/10.1021/ie201317u

Ross RD, Sheng H, Parihar A, Huang J, Jin S (2021) Compositionally tuned trimetallic thiospinel catalysts for enhanced electrosynthesis of hydrogen peroxide and built-in hydroxyl radical generation. ACS Catal 11(20):12643–12650. https://doi.org/10.1021/acscatal.1c03349

Serpone N, Artemev YM, Ryabchuk VK, Emeline AV, Horikoshi S (2017) Light-driven advanced oxidation processes in the disposal of emerging pharmaceutical contaminants in aqueous media: a brief review. Curr Opin Green Sustain Chem 6:18–33. https://doi.org/10.1016/j.cogsc.2017.05.003

Shang Y, Xu X, Gao B, Wang S, Duan X (2021) Single-atom catalysis in advanced oxidation processes for environmental remediation. Chem Soc Rev 50(8):5281–5322. https://doi.org/10.1039/D0CS01032D

Shi J, Ai Z, Zhang L (2014) Fe@Fe_2O_3 core-shell nanowires enhanced Fenton oxidation by accelerating the Fe(III)/Fe(II) cycles. Water Res 59:145–153. https://doi.org/10.1016/j.watres.2014.04.015

Sirés I, Brillas E, Oturan MA, Rodrigo MA, Panizza M (2014) Electrochemical advanced oxidation processes: today and tomorrow. A review. Environ Sci Pollut Res 21(14):8336–8367. https://doi.org/10.1007/s11356-014-2783-1

Song X, Zhang H, Bian Z, Wang H (2021) *In situ* electrogeneration and activation of H_2O_2 by atomic Fe catalysts for the efficient removal of chloramphenicol. J Hazard Mater 412:125162. https://doi.org/10.1016/j.jhazmat.2021.125162

Su P, Zhou M, Lu X, Yang W, Ren G, Cai J (2019) Electrochemical catalytic mechanism of N-doped graphene for enhanced H_2O_2 yield and *in-situ* degradation of organic pollutant. Appl Catal B 245:583–595. https://doi.org/10.1016/j.apcatb.2018.12.075

Su P, Zhou M, Song G, Du X, Lu X (2020) Efficient H_2O_2 generation and spontaneous •OH conversion for in-situ phenol degradation on nitrogen-doped graphene: pyrolysis temperature regulation and catalyst regeneration mechanism. J Hazard Mater 397:122681. https://doi.org/10.1016/j.jhazmat.2020.122681

Sun Y, Li Y, Mi X, Zhan S, Hu W (2019) Evaluation of ciprofloxacin destruction between ordered mesoporous and bulk $NiMn_2O_4$/CF cathode: efficient mineralization in a heterogeneous electro-Fenton-like process. Environ Sci Nano 6(2):661–671. https://doi.org/10.1039/C8EN01279B

Tang J, Wang J (2018) Metal organic framework with coordinatively unsaturated sites as efficient Fenton-like catalyst for enhanced degradation of sulfamethazine. Environ Sci Technol 52(9):5367–5377. https://doi.org/10.1021/acs.est.8b00092

Tang C, Wang H-F, Zhang Q (2018) Multiscale principles to boost reactivity in gas-involving energy electrocatalysis. Acc Chem Res 51(4):881–889. https://doi.org/10.1021/acs.accounts.7b00616

Wang J, Wang S (2019) Preparation, modification and environmental application of biochar: a review. J Clean Prod 227:1002–1022. https://doi.org/10.1016/j.jclepro.2019.04.282

Wang J, Wang S (2020) Reactive species in advanced oxidation processes: formation, identification and reaction mechanism. Chem Eng J 401:126158. https://doi.org/10.1016/j.cej.2020.126158

Wang Y, Zhao G, Chai S, Zhao H, Wang Y (2013) Three-dimensional homogeneous ferrite-carbon aerogel: one pot fabrication and enhanced electro-Fenton reactivity. ACS Appl Mater Interfaces 5(3):842–852. https://doi.org/10.1021/am302437a

Wang Y, Zou Y, Tao L, Wang Y, Huang G, Du S, Wang S (2019) Rational design of three-phase interfaces for electrocatalysis. Nano Res 12(9):2055–2066. https://doi.org/10.1007/s12274-019-2310-2

Wang J, Li S, Qin Q, Peng C (2021a) Sustainable and feasible reagent-free electro-Fenton via sequential dual-cathode electrocatalysis. Proc Natl Acad Sci 118(34):e2108573118. https://doi.org/10.1073/pnas.2108573118

Wang N, Ma S, Zuo P, Duan J, Hou B (2021b) Recent progress of electrochemical production of hydrogen peroxide by two-electron oxygen reduction reaction. Adv Sci 8(15):2100076. https://doi.org/10.1002/advs.202100076

Wang Y, Li W, Li H, Ye M, Zhang X, Gong C, Zhang H, Wang G, Zhang Y, Yu C (2021c) Fe/Fe_3C@CNTs anchored on carbonized wood as both self-standing anode and cathode for synergistic electro-Fenton oxidation and sequestration of As(III). Chem Eng J 414:128925. https://doi.org/10.1016/j.cej.2021.128925

Wang K, Zhao K, Qin X, Chen S, Yu H, Quan X (2022a) Treatment of organic wastewater by a synergic electrocatalysis process with Ti3+ self-doped TiO2 nanotube arrays electrode as both cathode and anode. J Hazard Mater 424:127747. https://doi.org/10.1016/j.jhazmat.2021.127747

Wang Y, Li S, Hou C, Jing L, Ren R, Ma L, Wang X, Wang J (2022b) Biomass-based carbon fiber/MOFs composite electrode for electro-Fenton degradation of TBBPA. Sep Purif Technol 282:120059. https://doi.org/10.1016/j.seppur.2021.120059

Wu P, Zhang Y, Chen Z, Duan Y, Lai Y, Fang Q, Wang F, Li S (2019) Performance of boron-doped graphene aerogel modified gas diffusion electrode for *in-situ* metal-free electrochemical advanced oxidation of Bisphenol A. Appl Catal B 255:117784. https://doi.org/10.1016/j.apcatb.2019.117784

Xiao F, Wang Z, Fan J, Majima T, Zhao H, Zhao G (2021a) Selective electrocatalytic reduction of oxygen to hydroxyl radicals via 3-electron pathway with FeCo alloy encapsulated carbon aerogel for fast and complete removing pollutants. Angew Chem Int Ed 60(18):10375–10383. https://doi.org/10.1002/anie.202101804

Xiao J, Chen J, Ou Z, Lai J, Yu T, Wang Y (2021b) N-doped carbon-coated Fe_3N composite as heterogeneous electro-Fenton catalyst for efficient degradation of organics. Chin J Catal 42(6):953–962. https://doi.org/10.1016/S1872-2067(20)63719-6

Xie L, Liu X, Chang J, Zhang C, Li Y, Zhang H, Zhan S, Hu W (2022) Enhanced redox activity and oxygen vacancies of perovskite triggered by copper incorporation for the improvement of electro-Fenton activity. Chem Eng J 428:131352. https://doi.org/10.1016/j.cej.2021.131352

Xu J, Zheng X, Feng Z, Lu Z, Zhang Z, Huang W, Li Y, Vuckovic D, Li Y, Dai S, Chen G, Wang K, Wang H, Chen JK, Mitch W, Cui Y (2021) Organic wastewater treatment by a single-atom catalyst and electrolytically produced H_2O_2. Nat Sustain 4(3):233–241. https://doi.org/10.1038/s41893-020-00635-w

Yan Q, Lian C, Huang K, Liang L, Yu H, Yin P, Zhang J, Xing M (2021) Constructing an acidic microenvironment by MoS2 in heterogeneous Fenton reaction for pollutant control. Angew Chem Int Ed 60(31):17155–17163. https://doi.org/10.1002/anie.202105736

Yang S, Verdaguer-Casadevall A, Arnarson L, Silvioli L, Čolić V, Frydendal R, Rossmeisl J, Chorkendorff I, Stephens IEL (2018a) Toward the decentralized electrochemical production of H_2O_2: a focus on the catalysis. ACS Catal 8(5):4064–4081. https://doi.org/10.1021/acscatal.8b00217

Yang W, Zhou M, Liang L (2018b) Highly efficient *in-situ* metal-free electrochemical advanced oxidation process using graphite felt modified with N-doped graphene. Chem Eng J 338:700–708. https://doi.org/10.1016/j.cej.2018.01.013

Yang W, Zhou M, Oturan N, Li Y, Su P, Oturan MA (2019) Enhanced activation of hydrogen peroxide using nitrogen doped graphene for effective removal of herbicide 2,4-D from water by iron-free electrochemical advanced oxidation. Electrochim Acta 297:582–592. https://doi.org/10.1016/j.electacta.2018.11.196

Yang X, Chen Z, Du S, Meng H, Ren Z (2022) Cu-coupled Fe/Fe3C covered with thin carbon as stable win-win catalysts to boost electro-Fenton reaction for brewing leachate treatment. Chemosphere 293:133532. https://doi.org/10.1016/j.chemosphere.2022.133532

Yao B, Luo Z, Yang J, Zhi D, Zhou Y (2021) $Fe^{II}Fe^{III}$ layered double hydroxide modified carbon felt cathode for removal of ciprofloxacin in electro-Fenton process. Environ Res 197:111144. https://doi.org/10.1016/j.envres.2021.111144

Yu F, Zhou M, Zhou L, Peng R (2014) A novel electro-fenton process with H_2O_2 generation in a rotating disk reactor for organic pollutant degradation. Environ Sci Technol Lett 1(7):320–324. https://doi.org/10.1021/ez500178p

Yu Q, Feng L, Chai X, Qiu X, Ouyang H, Deng G (2019) Enhanced surface Fenton degradation of BPA in soil with a high pH. Chemosphere 220:335–343. https://doi.org/10.1016/j.chemosphere.2018.12.141

Yu D, He J, Wang Z, Pang H, Li L, Zheng Y, Chen Y, Zhang J (2021a) Mineralization of norfloxacin in a CoFe–LDH/CF cathode-based heterogeneous electro-fenton system: Preparation parameter optimization of the cathode and conversion mechanisms of H_2O_2 to ·OH. Chem Eng J 417:129240. https://doi.org/10.1016/j.cej.2021.129240

Yu M, Dong H, Liu K, Zheng Y, Hoffmann MR, Liu W (2021b) Porous carbon monoliths for electrochemical removal of aqueous herbicides by "one-stop" catalysis of oxygen reduction and H_2O_2 activation. J Hazard Mater 414:125592. https://doi.org/10.1016/j.jhazmat.2021.125592

Zhang H, Liu G, Shi L, Ye J (2018) Single-atom catalysts: emerging multifunctional materials in heterogeneous catalysis. Adv Energy Mater 8(1):1701343. https://doi.org/10.1002/aenm.201701343

Zhang Q, Zhou M, Ren G, Li Y, Li Y, Du X (2020) Highly efficient electrosynthesis of hydrogen peroxide on a superhydrophobic three-phase interface by natural air diffusion. Nat Commun 11(1):1731. https://doi.org/10.1038/s41467-020-15597-y

Zhang D, Yin K, Tang Y, Wei Y, Tang H, Du Y, Liu H, Chen Y, Liu C (2022a) Hollow sea-urchin-shaped carbon-anchored single-atom iron as dual-functional electro-Fenton catalysts for degrading refractory thiamphenicol with fast reaction kinetics in a wide

pH range. Chem Eng J 427:130996. https://doi.org/10.1016/j.cej.2021.130996

Zhang J, Qiu S, Feng H, Hu T, Wu Y, Luo T, Tang W, Wang D (2022b) Efficient degradation of tetracycline using core–shell Fe@Fe_2O_3-CeO_2 composite as novel heterogeneous electro-Fenton catalyst. Chem Eng J 428:131403. https://doi.org/10.1016/j.cej.2021.131403

Zhao H, Qian L, Guan X, Wu D, Zhao G (2016a) Continuous bulk FeCuC aerogel with ultradispersed metal nanoparticles: an efficient 3D heterogeneous electro-Fenton cathode over a wide range of pH 3–9. Environ Sci Technol 50(10):5225–5233. https://doi.org/10.1021/acs.est.6b00265

Zhao S, Wang Y, Zhang Q, Li Y, Gu L, Dai Z, Liu S, Lan Y-Q, Han M, Bao J (2016b) Two-dimensional nanostructures of non-layered ternary thiospinels and their bifunctional electrocatalytic properties for oxygen reduction and evolution: the case of $CuCo_2S_4$ nanosheets. Inorganic Chem Front 3(12):1501–1509. https://doi.org/10.1039/C6QI00355A

Zhao H, Qian L, Chen Y, Wang Q, Zhao G (2018) Selective catalytic two-electron O_2 reduction for onsite efficient oxidation reaction in heterogeneous electro-Fenton process. Chem Eng J 332:486–498. https://doi.org/10.1016/j.cej.2017.09.093

Zhao K, Quan X, Su Y, Qin X, Chen S, Yu H (2021) Enhanced chlorinated pollutant degradation by the synergistic effect between dechlorination and hydroxyl radical oxidation on a bimetallic single-atom catalyst. Environ Sci Technol 55(20):14194–14203. https://doi.org/10.1021/acs.est.1c04943

Zhou W, Rajic L, Chen L, Kou K, Ding Y, Meng X, Wang Y, Mulaw B, Gao J, Qin Y, Alshawabkeh AN (2019) Activated carbon as effective cathode material in iron-free Electro-Fenton process: integrated H_2O_2 electrogeneration, activation, and pollutants adsorption. Electrochim Acta 296:317–326. https://doi.org/10.1016/j.electacta.2018.11.052

Zhou X, Xu D, Chen Y, Hu Y (2020) Enhanced degradation of triclosan in heterogeneous E-Fenton process with MOF-derived hierarchical Mn/Fe@PC modified cathode. Chem Eng J 384:123324. https://doi.org/10.1016/j.cej.2019.123324